ION MODULATED ORGANIC TRANSISTORS

Nikolai Kaihovirta

Physics
Department of Natural Sciences
Center for Functional Materials
Graduate School of Materials Research
Åbo Akademi University
Åbo 2010

ION MODULATED ORGANIC TRANSISTORS

Nikolai Kaihovirta

Physics
Department of Natural Sciences
Center for Functional Materials
Graduate School of Materials Research
Åbo Akademi University
Åbo 2010

Supervisor:

Prof. Ronald Österbacka
Åbo Akademi University

Pre-examiners:

Prof. Ludvig Edman
Umeå University

Dr. Thomas D. Anthopoulos
Imperial College London

Opponent for the public defense:

Prof. C. Daniel Frisbie
University of Minnesota

ISBN 978-952-12-2468-3
Painosalama Oy, Turku, Finland 2010

PREFACE

This thesis comprises research conducted on ion modulated organic transistors during 2006 – 2010 at the organic electronics group in the Department of Physics at ÅA. The reported results are achieved through interaction and collaboration with a number of colleagues (both within Physics as well as interdisciplinary), to whom I am sincerely grateful.

Late in 2005, I was asked by Prof. Ronald Österbacka to start working with organic electronics. Ronald also became my supervisor and I am thankful for all the great discussions and the inspiration he has provided me. I was handed the independence, as well as the responsibility, to master my research within the theme. By this arrangement, I have obtained qualities that I will highly appreciate in my future career as a researcher. When I started to work in 2006, I had no previous background from organic electronics. Dr. Tomas Bäcklund served as my mentor the first months, for which I am very grateful.

The work together with colleagues at the Laboratory of Polymer Technology at ÅA has been essential for many of the results in this thesis. I consider that our collaboration has been ideal: open discussions on a regular basis, innovative ideas and purposeful work towards a common target and by utilizing each others expertise. Therefore, I wish to acknowledge Prof. Carl-Eric Wilén, Carl-Johan Wikman and Xuehan He for this and also for helping me comprehend polymer chemistry.

In my eyes, the articles enclosed in this thesis clearly display a positive development in my reporting skills. I have elaborated my writing by carefully reading scientific publications written by others. However, I have also gained invaluable help and assistance from many of my colleagues at the organic electronics group. I particularly wish to thank Dr. Tapio Mäkelä, Dr. Himadri Majumdar, Harri Aarnio and Daniel Tobjörk for excellent collaboration and for stimulating discussions.

The help from Dr. Kjell-Mikael Källman, our laboratory engineer, can never be exaggerated. He is very much responsible for that our ideas and hypotheses (irrespective of how crazy they may be) can be tried out in the lab. Also, I should not omit acknowledging Dr. Kaj Höglund for all the enjoyable discussions and for the much appreciated practical advices around this work. Furthermore, I wish to thank all the colleagues at the Department of Physics for keeping up such a pleasant atmosphere.

Off work, my family and my friends have always been important for me. Till mina föräldrar Ingrid och Ilkka: Fastän forskningen emellanåt har verkat svår att begripa, har ert villkorslösa stöd varit oerhört betydelsefullt för mig.

Finally, I wish to thank my Hannis for all the love and support that you are giving me.

August 15, 2010
Åbo

CONTENTS

OUTLINE OF THESIS

The transistor is one of the greatest technological innovations of the 20th century. The switching and/or signal amplifying properties are utilized in most inorganic electronic applications and a single microprocessor may contain billions of transistors. Polymeric materials provide solubility, flexibility and low cost into transistors, in particular. On the other hand, the slower switching speeds and the lower integration density for organic transistors will prevent them from competing with the established inorganic transistors. The previous work on the low-voltage (< 3 V) hygroscopic insulator field-effect transistor (HIFET), achieved in our laboratory by T. G. Bäcklund, et. al., has served as a starting-point for this work. The targets were to continue the research on the HIFET towards large-scale manufacturing, to improve our knowledge on ion modulated organic transistors (both electrolyte gated organic field-effect transistors (OFETs) and organic electrochemical transistors (ECTs)) and to develop novel concepts by utilizing ion-conducting membranes.

The thesis is based on five papers and constitutes of two parts. Part I is, furthermore, divided into four chapters. In Chapter 1, a comprehensive theory on the organic transistors is provided, with particular focus on the traditional OFET. The same theory can be directly applied on the electrolyte gated OFETs as well, which is the central transistor type in this thesis. The experimental details are covered in Chapter 2. Chapter 3 highlights the most important findings and discussions based on the five papers, while Chapter 4 provides a summary of this thesis. The five papers are attached in Part II.

The research in this thesis has been done within the Center for Functional Materials (FUNMAT) and Graduate School of Materials Research (GSMR). FUNMAT is a joint research center between laboratories from Physics, Polymer Technology, Physical Chemistry and Paper Coating and Converting in Åbo Akademi University as well as Polymer Chemistry in University of Helsinki. The strategy for FUNMAT is to develop materials, routes and devices towards printed functionalities by combining the know-how from the participating laboratories. FUNMAT was funded by Åbo Akademi Foundation 2006 – 08 and is, from 2008 onwards, a National Center of Excellence. GSMR combines 13 laboratories from both Åbo Akademi University and

University of Turku that are involved in material research and material technology.

Papers 3, 4 and 5 have, furthermore, been done within the "Novel technology platform for mass produced inexpensive transistors on flexible substrates enabling sensing applications" (FLEXSENS) project, which is financed by the Finnish Funding Agency for Technology and Innovation (TEKES) and by some industrial partners. In FLEXSENS participates all the FUNMAT laboratories from Åbo Akademi University as well as laboratories from Oulu University, Tampere University of Technology and University of Turku.

LIST OF INCLUDED PUBLICATIONS

1. **Absence of substrate roughness effects on an all-printed organic transistor operating at one volt**
   Nikolai J. Kaihovirta, Daniel Tobjörk, Tapio Mäkelä, and Ronald Österbacka
   Applied Physics Letters, **93**, 053302 (2008).

2. **Self-Supported Ion-Conductive Membrane-Based Transistors**
   Nikolai J. Kaihovirta, Carl-Johan Wikman, Tapio Mäkelä, Carl-Eric Wilén, and Ronald Österbacka
   Advanced Materials, **21**, 2520-2523 (2009).

3. **Printed all-polymer electrochemical transistors on patterned ion conducting membranes**
   Nikolai Kaihovirta, Tapio Mäkelä, Xuehan He, Carl-Johan Wikman, Carl-Eric Wilén, and Ronald Österbacka
   Organic Electronics, **11**, 1207-1211 (2010).

4. **The Effects of Moisture in a Low-Voltage Organic Field-Effect Transistor Gated with a Hydrous Solid Electrolyte**
   Nikolai Kaihovirta, Harri Aarnio, Carl-Johan Wikman, Carl-Eric Wilén, and Ronald Österbacka
   Advanced Functional Materials, **20**, 2605-2610 (2010).

5. **Improved device stability by adding a sterically hindered phenolic antioxidant in low-voltage organic field-effect transistors**
   Nikolai Kaihovirta, Carl-Johan Wikman, Harri Aarnio, Carl-Eric Wilén, and Ronald Österbacka
   Submitted (2010)

AUTHOR´S CONTRIBUTION

The contribution of the author to the publications included in this thesis is the following:

Paper 1. The author prepared all solutions and all the transistors that were fabricated by spin-coating. The author did all the electrical characterizations and the atomic force microscopy studies. Furthermore, the author wrote the manuscript and finalized it together with the co-authors.

Paper 2. The author prepared the semiconductor solutions and fabricated the transistors and the electrochromic devices. The author did all the electrical characterizations. Furthermore, the author wrote the manuscript and finalized it together with the co-authors.

Paper 3. The author prepared the solutions and designed the masks for the flexographic printing. The author did all the electrical characterizations. Furthermore, the author wrote the manuscript and finalized it together with the co-authors.

Paper 4. The author prepared the semiconductor solutions and fabricated all samples. The author did all electrical characterizations, except for the impedance spectroscopy measurements, and contributed equally in the optical measurements together with Harri Aarnio. Furthermore, the author wrote the manuscript and finalized it together with the co-authors.

Paper 5. The author prepared the semiconductor solutions and fabricated all samples. The author did the UV-Vis analysis and all electrical characterizations. Furthermore, the author wrote the manuscript and finalized it together with the co-authors.

RELATED PUBLICATIONS

1. **Low-Voltage All-Polymer Transistors**
   In: D. K. Aswal, J. V. Yakhmi (Eds.), Molecular and Organic Electronic Devices. Nova Science Publishers, Inc., Hauppauge, NY (2010) in press.

2. **Components and circuit arrangements including at least one organic field-effect transistor**
   Ronald Österbacka, Carl-Eric Wilén, Nikolai Kaihovirta, Carl-Johan Wikman, and Tapio Mäkelä
   Patent WO 2010/010233 A1

3. **An organic field-effect transistor**
   Ronald Österbacka, Carl-Eric Wilén, Tomas Bäcklund, and Nikolai Kaihovirta
   Patent WO 2008/090257 A1

4. **A multilayer coated fiber-based substrate suitable for printed functionality**
   Roger Bollström, Anni Määttänen, Daniel Tobjörk, Petri Ihalainen, Nikolai Kaihovirta, Ronald Österbacka, Jouko Peltonen, and Martti Toivakka
   Organic Electronics, **10**, 1020-1023 (2009).

5. **All-printed low-voltage organic transistors**
   Daniel Tobjörk, Nikolai J. Kaihovirta, Tapio Mäkelä, Fredrik S. Petersson, and Ronald Österbacka
   Organic Electronics, **9**, 931-935 (2008).

6. **Low-Voltage Organic Transistors Fabricated Using Reverse Gravure Coating on Prepatterned Substrates**
   Nikolai J. Kaihovirta, Daniel Tobjörk, Tapio Mäkelä, and Ronald Österbacka
   Advanced Engineering Materials, **10**, 640-643 (2008).

Part I. SYNOPSIS

1. INTRODUCTION

This chapter provides a brief motivation to organic electronics research in general, and to the research on organic transistors in particular. The essential theory on organic field-effect transistors (OFETs) is given in Sections 1.2.1 and 1.2.2. Three types of organic transistors are defined in this thesis. The differences between the transistor-types are discussed in Section 1.2.3. Parts of the theory in Chapter 1 (and in Chapter 2) have also been presented in a book-chapter by N. Kaihovirta and R. Österbacka [Related Publication 1.].

1.1 Background

Ever since the first **trans**fer res**istor** (transistor) operation was demonstrated in 1948 [1], tremendous development in the field of electronics has been achieved. A significant milestone for integrated circuits technology was the invention of the metal oxide semiconductor field-effect transistor (MOSFET) [2], which has also been important for the organic electronics research. In 1977, the first report on a dramatic conductivity enhancement in doped poly(acetylene) was presented [3] that eventually resulted in the Nobel prize in chemistry in the year 2000. The first organic transistor functionality, based on solid-state electrochemical reduction and oxidation (redox) of poly(pyrrole), was demonstrated by White, et. al. in 1984 [4]. In 1986, Tsumura, et. al. were one of the first groups to demonstrate an organic field-effect transistor (OFET) by using poly(thiophene) as the polymeric semiconductor [5]. The research on organic transistors has been focusing on understanding material properties, utilizing novel materials and on resolving challenges, such as improving the device operation efficiency as well as enhancing the life-time and the environmental stability. Particularly π-conjugated semiconducting and conducting polymers have been interesting due to their possibility of being casted from solution. These materials are also flexible, and in conjunction with traditional (insulating) polymers they enable the possibility of large-scale manufacturing of organic electronic devices at low cost. Furthermore, the compatibility of conducting polymers with biosystems has also resulted in novel innovations, such as

electrochemical sensors, micro-fluidic systems and drug delivery devices [6]. In other words, organic bioelectronics is an area of research that displays the potential for polymeric materials.

A high-performing transistor should provide a high on-current at low voltages. For a field-effect transistor (MOSFET and OFET) this sets a requirement to the capacitance (C) of the dielectric insulator:

$$C_i = \frac{C}{A} = \frac{\kappa\varepsilon_0}{d}, \qquad (1.1)$$

where C_i is the effective capacitance (capacitance per unit area), κ is the dielectric constant of the insulator, ε_0 is the vacuum permittivity and d is the insulator thickness. According to Equation (1.1), there are basically two ways of increasing C_i: (1) By decreasing the insulator thickness, or (2) by increasing the dielectric constant. High performing, low-voltage (< 5 V) OFETs have been demonstrated with both alternatives. On the other hand, it is challenging to reach low-voltage operation with OFETs and still maintain robustness, stability and flexibility of the structure. Another route has therefore been to replace the ordinary (dielectric) insulator with an ion-conducting insulator (e.g., an electrolyte) to construct either electrolyte gated OFETs or organic electrochemical transistors (ECTs). In this thesis, both transistor types are defined as ion modulated organic transistors. The electrolyte gated OFET, which is the central type in this thesis, uses the same transistor structures and follows the same current-voltage (I-V) analysis as the conventional OFET.

1.2 The OFET and the Ion Modulated Organic Transistors

1.2.1 Transistor Structures

The OFET constitutes of thin films fabricated as subsequent layers. The polymeric materials are often soluble (or dispersible) in common organic solvents, and are, therefore, easily processed by drop-casting, spin-coating and/or by various large-scale coating and printing techniques. The thickness range of each layer may vary from a few tens of nanometers up to several micrometers. The OFET is a three-terminal device with a source, drain and a gate electrode. The electronic current path (the active channel) is formed between the source and drain at the

semiconductor/insulator interface. The active channel is only a few monolayers thick. The active channel is furthermore separated from the gate by an insulator. The four basic OFET-structures are shown in Figure 1.1. These are either top-contact (Figures 1.1 (a) and (b)) or bottom-contact (Figures 1.1 (c) and (d)). Furthermore, the transistor structure also depends on the placement of the gate. It can be either in the bottom-gate (Figures 1.1 (a) or (c)) or in the top-gate configuration (Figures 1.1 (b) and (d)).

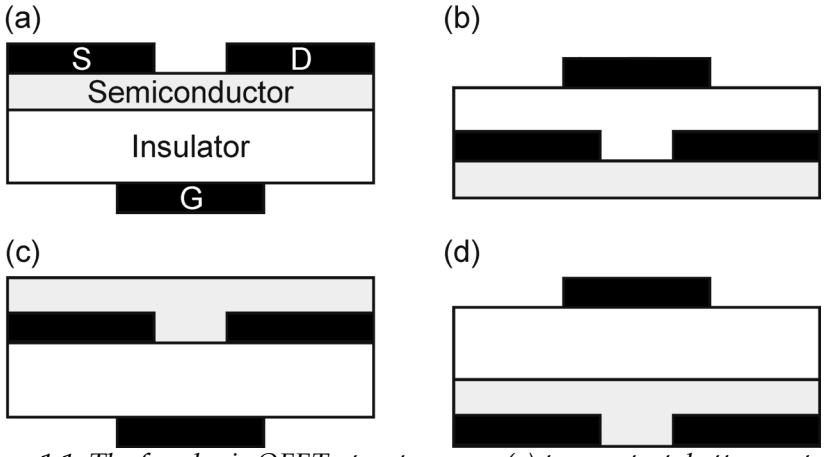

Figure 1.1. The four basic OFET-structures are (a) top-contact, bottom-gate, (b) top-contact, top-gate, (c) bottom-contact, bottom-gate, and (d) bottom-contact top-gate.

An OFET-structure should meet a few criteria. Firstly, it is crucial for the gate to be aligned directly underneath/over the active channel, in order to avoid stray capacitances or edge effects. Secondly, the layers applied in a consecutive fashion demand the use of solvents that do not dissolve the underlying layer and/or increase the roughness at the interfaces. This is particularly crucial at the active channel interface. Thirdly, the current output is dependent on the choice of device geometry. The top-contact, bottom-gate (Figure 1.1 (a)) and the bottom-contact, top-gate (Figure 1.1 (d)) geometries benefit from a larger injection area, which would result in a lower contact resistance [7]. However, the injected charges need to travel through an undoped region of the semiconductor in order to reach the active channel [8, 9], and therefore the thickness of the semiconductor layer becomes a significant parameter. Furthermore, it has been shown that the injection area is not unambiguously defined by the gate overlapping area [9]. This, so called, current crowding effect, implies that the charge injection from the source

mostly occurs at the edge of the source, due to the horizontal electric field created between the source and drain.

1.2.2 Current-Voltage Analysis

Since the thesis only concerns with p-channel (hole conducting) polymeric semiconductors, the following theory is applied for p-channel OFETs. However, the theory is analogous for n-channel (electron conducting) OFETs upon switching the polarity of the applied voltages.

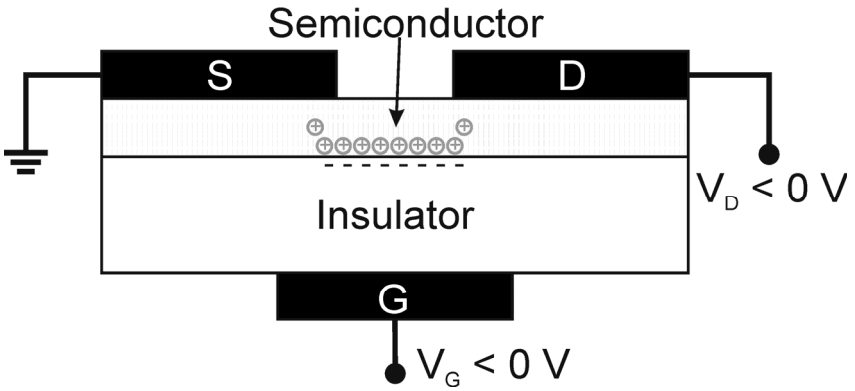

Figure 1.2.The bias-scheme for a p-channel OFET. The active channel is situated at the semiconductor/insulator interface.

For the p-channel OFET, the drain is biased negatively towards the source, in order to inject holes from the source. The conductivity, in the active channel, is modulated by the gate under the influence of the electric field over the dielectric insulator (Figure 1.2). The most common *I-V* characteristics are the output- (I_{DS}-V_{DS}) and transfer-curves (I_{DS}-V_G), also shown in Figure 1.3. In the output-curve, the drain-voltage (V_{DS}) is swept at different gate-voltage (V_G) steps. Thus, the accumulated charges in the active channel modulate the drain-current (I_{DS}). The output-curve can be divided into two regions (Figure 1.3 (a)), namely the linear ($V_{DS} << V_G$) and the saturated region ($V_{DS} > V_G$). The linear region situates between the threshold voltage (V_T) and the pinch-off point, in which I_{DS} increases linearly. In this region, the active channel is formed at V_T, and the current is not limited by the charge concentration, that is, the current has an ohmic behavior. I_{DS} can be analytically expressed as:

$$I_{DS} = \frac{W}{L}\mu C_i\left(V_G - V_T - \frac{V_{DS}}{2}\right)V_{DS}, \quad (1.2)$$

where W and L is the channel width and length, and μ is the charge mobility. By assuming $V_{DS} << V_G$, and by taking the derivative of Equation (1.2) with respect to V_{DS}, the channel conductance (g_D) is defined:

$$\frac{\partial I_{DS}}{\partial V_{DS}} \equiv g_D = \frac{W}{L}\mu C_i\left(V_G - V_T\right). \quad (1.3)$$

At $V_{DS} = V_G$, the charges, close to the drain, become depleted, and I_{DS} will be "pinched off". Thus, the current is saturated. For the saturated current, an analytical expression is obtained, when assuming that the current level remains constant after the pinch-off point ($V_{DS} = V_G$):

$$I_{DS} = \frac{W}{2L}\mu C_i\left(V_G - V_T\right)^2. \quad (1.4)$$

From Equation (1.3) it naturally follows, that the channel conductance $g_D = 0$, in the saturated region. It is noteworthy that Equations (1.2) and (1.4) are valid only if the charge concentration in the active channel is controlled by the vertical electric field, induced by the gate. As a rule of thumb, this holds for channel lengths $L > 4d$ [10-12], where d is the thickness of the insulator. A certain degree of variation in the L-d dependence exists, for instance, due to the source and drain electrodes, the thinness of the insulator and due to the used semiconductor [13]. For shorter channel lengths the horizontal electric field dominates and short-channel effects emerge. Typically, the short-channel effect results in a non-saturated I_{DS} after pinch-off, that is, $g_D \neq 0$ in the saturated region.

In the transfer-characteristics (Figure 1.3 (b)) V_G is swept, while V_{DS} is kept constant either in the linear region or in the saturated region. While the output-curve is characterized (almost) at constant accumulation, the transfer-curve is swept over a broader accumulation range. Therefore, the transfer-curve provides thorough information of the switching property, stability and charge mobility of the transistor. The on/off ratio measures the current ratio between the on-state and the off-state. A high on/off ratio is naturally desired, in order to have a distinctive on- and off-state. Based on amorphous silicon (a-Si) MOSFETs, the requirement for high performing OFETs are on/off ratios exceeding 10^6. The slope of the transfer-curve, after V_T, is denoted as the subthreshold slope (S). The subthreshold slope determines the sharpness of the transition from off- to on-state, and is defined in units of [V/decade]. A lower S implicates a faster switch. Often the turn-on voltage (V_0) is also extracted from the

transfer-curve. V_0 is defined as the voltage where the transistor turns from the off-state to the subthreshold region, see Figure 1.3 (b). Although related, V_0 should, however, not be confused with V_T, which has a direct physical definition as described above.

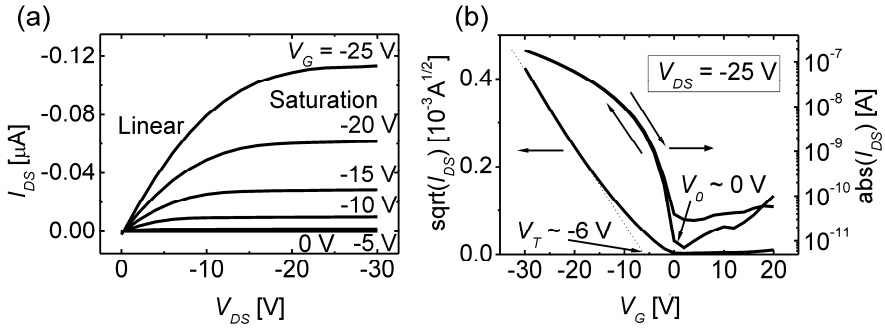

Figure 1.3. (a) Output- and (b) transfer-characteristics for a p-channel OFET. The transfer-curve is measured in the saturated region. The square-root of I_{DS} is also shown in (b).

The transfer-curve can be swept both forward and back to determine any hysteresis. The hysteresis is generally a result of trapped charges at the active channel/insulator, but also possible ionic drift, in the insulator, may cause hysteresis. Another important parameter is the charge mobility (μ). Basically, μ illustrates how fast charges move through the active channel and can be derived from Equations (1.2) and (1.4) with respect to V_G. In the linear region this would be:

$$\frac{\partial I_{DS}}{\partial V_G} \equiv g_m = \frac{W}{L}\mu C_i V_{DS}, \qquad (1.5)$$

where g_m is the transconductance. From Equation (1.5), μ can be obtained:

$$\mu = \frac{\partial I_{DS}}{\partial V_G}\frac{L}{WC_i V_{DS}}. \qquad (1.6)$$

Similarly for I_{DS} in the saturated regime (Equation (1.4)):

$$\frac{\partial I_{DS}}{\partial V_G} \equiv g_m = \frac{W}{L}\mu C_i (V_G - V_T), \qquad (1.7)$$

and μ will be:

$$\mu = \frac{\partial I_{DS}}{\partial V_G} \frac{L}{WC_i (V_G - V_T)}. \qquad (1.8)$$

Analogously, μ can be extracted from the transfer-curve. For example, in Figure 1.3 (b), the square-root of I_{DS} is plotted with respect to V_G. According to Equation (1.4) (because the transfer-curve is measured in the saturated region):

$$\sqrt{I_{DS}} = \sqrt{\frac{WC_i \mu}{2L}} (V_G - V_T). \qquad (1.9)$$

A re-arrangement of the terms yields:

$$\mu = \frac{2Lk^2}{WC_i}, \qquad (1.10)$$

where k is the slope of the curve, as indicated by the black line in Figure 1.3 (b). The threshold voltage (V_T) is obtained by extrapolating the slope of the square-root of I_{DS} to the intersection of the x-axis.

Finally, it should be noted that μ is assumed constant at all voltages in Equations (1.2) and (1.4). However, μ varies at different V_G's for OFETs (especially in OFETs using amorphous semiconductors) due to the hopping transport in a broad Gaussian density of localized states [14]. Consequently, given a mobility value, the charge concentration should also be given.

1.2.3 Three Types of Organic Transistors

Because of the low power consumption and wide application area of the inorganic MOSFETs, **the OFETs** have naturally become the most studied type out of the three organic transistor types. Typically, low-voltage OFETs have either adopted various oxides as high-κ insulators [15-17], ultra-thin cross-linked polymers [10-12, 18-20] and/or self-assembled monolayers [21-23] as low-d insulators (<< 100 nm), in order to fulfill the requirements set by Equation (1.1). However, these alternatives are often either brittle, non-flexible, susceptible to pin-holes, cracks and electrical breakdown, sensitive to surface roughness and/or require high-temperature processing. Therefore, low-cost and large-area fabrication of low-voltage OFETs is challenging.

It is known that doping of the polymeric semiconductor by using an electrolyte results in a transition to metallic-like properties for the polymer [24, 25]. In the **electrolyte gated OFET** the dielectric insulator is replaced by an electrolyte "insulator". One of the first demonstrated electrolyte gated OFETs was the hygroscopic insulator field-effect transistor (HIFET) [26]. As emphasized by its name, the HIFET uses a polymeric insulator that becomes ion-conducting when exposed to small protic solvents, such as moisture. In such an environment, the HIFET operates as an electrolyte gated OFET.

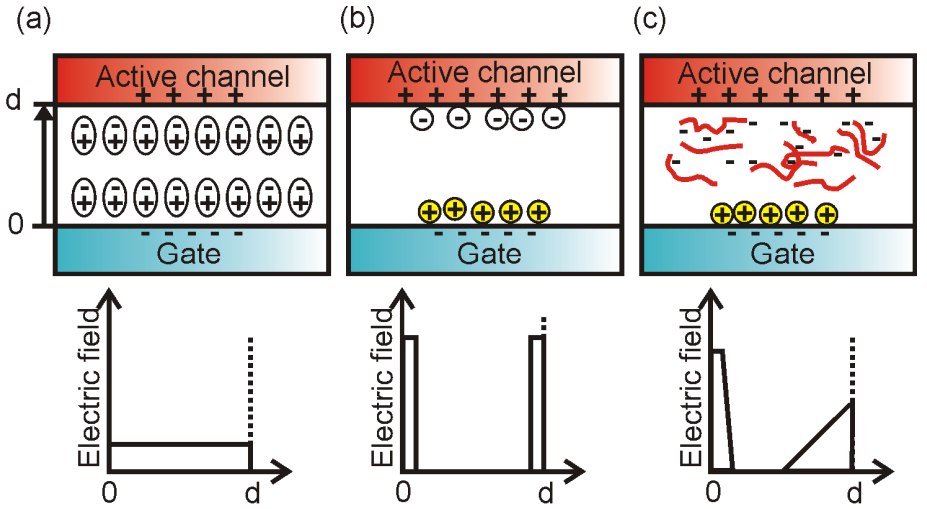

Figure 1.4. A schematic representation of the charge polarization and on how the electric field would distribute in OFETs gated by (a) a dielectric, (b) an electrolyte where the counter-ions are equally large, and (c) an electrolyte constituting of cations and immobile polyanions.

In the electrolyte "insulator", a gate potential will cause anions and cations to migrate towards opposite interfaces of the electrolyte. For a p-channel transistor, the applied negative gate voltage assembles anions at the vicinity of the electrolyte/semiconductor interface and, correspondingly, cations at the electrolyte/gate interface, as schematically illustrated in Figure 1.4. In the simplest model (Figure 1.4 (b)), where the counter-ions are equally large and mobile, the ionic re-orientation creates equal electric double layers (EDLs) at respective interfaces. The electric field in the bulk of the electrolyte is zero. Therefore, unlike the dielectric insulator, the capacitance is independent to the thickness of the insulator [27]. Instead, the capacitance of the electrolyte is the sum of the capacitances for both EDLs:

$$C_{Electrolyte} = \frac{C_{EDL1} C_{EDL2}}{C_{EDL1} + C_{EDL2}}. \qquad (1.11)$$

In the simplest model $C_{EDL1} = C_{EDL2}$, that is, $C_{Electrolyte} = 1/2\ C_{EDL1}$. Ideally, the thickness of the EDLs is on the order of Ångströms. Hence, the resulting C_i can be 10 - 100 μF/cm², which exceeds the capacitance of ordinary dielectric insulators by several orders of magnitude. Unlike the OFET (Section 1.2.1), the ionic drift allows for the gate to be unaligned relative to the active channel [28, 29]. This naturally simplifies device fabrication. On the other hand, it also creates additional problems, for example, concerning cross-talk between neighboring transistors.

Small and mobile ions also enhance the risk for electrochemical interaction with the polymeric semiconductor. Most π-conjugated polymers are redox-active. At a threshold gate potential, anions will penetrate the electrolyte/semiconductor interface and electrochemically dope the semiconductor [30, 31]. Thus, the doping of the semiconductor changes from an interfacial effect to a bulk effect. Electrochemical doping of the polymeric semiconductor will result in a structural and electronic perturbation that can be either reversible [30, 31] or irreversible (Paper 4). In both scenarios, electrochemical doping of the polymeric semiconductor will inevitably slow down the switching response of the transistor. However, if the transistor operation is durable and steady for a longer period of time, then it is less important whether the doping of the polymeric semiconductor is governed by field-effect or electrochemistry. Furthermore, for a fast polarizable electrolyte an increase in the switching frequency will reduce ionic penetration into the semiconductor that will minimize electrochemical interaction [31].

By utilizing an immobile anion, the problems associated with electrochemical doping may be circumvented. The anion can be covalently bound to a polymer (polyanion) [28, 32]. In such cases, the counter-ions are not equal in size and mobility, and the polyanionic EDL will be distributed over a broader region, as illustrated in Figure 1.4 (c). For example, according to Equation (1.11), if $C_{EDL2} = 10\ C_{EDL1}$, then $C_{Electrolyte}$ would be $C_{Electrolyte} = 10/11\ C_{EDL1} \approx C_{EDL1}$. Consequently, the capacitance of the electrolyte is dominated by its smallest term, which would be the capacitance over the polyanionic EDL. Indeed, lower C_i´s are measured for polyelectrolytes albeit the low-voltage operation usually is preserved, which will be shown in Chapter 3.

$$PEDOT^{+}PSS^{-} + M^{+} + e^{-} \rightleftharpoons PEDOT^{0} + M^{+}PSS^{-}$$

Scheme 1.1. The reversible redox-reaction for the conducting polymeric dispersion PEDOT/PSS.

Organic ECTs were developed in the mid- and late-eighties as a result of thorough research on the redox-reaction of various π-conjugated polymers [4, 33-37]. Usually, the device structure is similar to the OFET-structure with the source and drain electrodes connected by a π-conjugated polymer. The gate is furthermore separated from the active interface by an electrolyte. However, unlike the OFET and the electrolyte gated OFET, the *I-V* analysis described in Section 1.2.2 does not apply for the ECT. The electronic conductivity through the transistor channel (i.e., the part of the π-conjugated polymer, which is covered by the electrolyte [38]) is electrochemically controlled by reducing/oxidizing the π-conjugated polymer throughout the bulk. In Scheme 1.1, for example, the reversible redox-reaction is shown for the conducting polymeric dispersion poly(ethylene dioxythiophene)/polystyrene sulfonic acid (PEDOT/PSS). The difference in the electronic conductivity between the high-conducting $PEDOT^{+}$ and the low-conducting $PEDOT^{0}$ can be several orders of magnitude [38]. Figure 1.5 illustrates an electrochemical cell comprised by the polymeric gate, the electrolyte and the transistor channel. The counter-ions (M^{+}) are provided by the electrolyte. If neglecting any possible electronic leakage and chemical side-reactions, then the number of charges participating in the redox-reaction can be estimated by:

$$Q = \int_{0}^{t_f} I_G dt\,, \qquad (1.13)$$

where Q is the charge, t is the time and t_f is the time at the end of the redox-reaction. Thus, the switching between the on- and off-state in the ECT is time-dependent. Furthermore, the switching is governed by the ionic properties of the electrolyte (bulkiness of the ions, ionic conductivity and mobility, etc) as well as by the ionic transport within the π-conjugated polymer. On the other hand, due to the redox-mechanism the organic ECT can be built in a lateral configuration (apart from the vertical geometries shown in Figure 1.1). Furthermore, the device is insensitive to surface roughness [38], especially compared to OFETs. It is noteworthy that the gate electrode (as well as the source and drain electrodes) can also be metallic as long as the transistor channel is redox-active [4, 33-37]. Organic ECTs have particularly been studied for sensory applications,

due to their ability of transducing an ionic signal to an electronic signal [39-41].

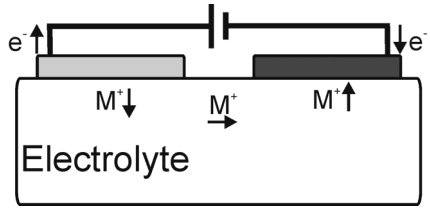

Figure 1.5. The electrochemical cell can be used to describe the redox-reaction between the transistor channel/electrolyte and the gate/electrolyte.

2. EXPERIMENTAL

This chapter reviews the polymeric materials and experimental procedures that were routinely used throughout this thesis. The most essential characterization techniques are described in Section 2.2.

2.1 Materials and Methods

2.1.1 Substrates

High performing OFETs are usually manufactured on rigid and smooth substrates such as silicon. However, in order to fully exploit the benefits of polymeric materials, the choice of inexpensive and flexible substrates such as plastic and paper must be considered. These substrates are suitable for roll-to-roll fabrication, and the transparency of the plastic substrate is beneficial for novel applications. On the other hand, the plastic and paper substrates provide challenges, for instance, with increased physical roughness, liquid sorption and poor chemical resistance. These obstacles may be overcome by applying a planarizing layer and/or a barrier layer [42]. Another challenge is the low processing temperatures (< 300 °C) of plastic and paper substrates that efficiently hinders fabrication of inorganic transistors onto these substrates.

The polyester-type substrate poly(ethylene terephtalate) (PET)-film (Chart 2.1 a)) had previously been used for fabricating HIFETs [26, 27]. It was, therefore, a natural choice as a plastic substrate for continuing work towards the all-printed HIFET (Paper 1). In the HIFET, the only purpose for the plastic substrate is to support the transistor structure. The most frequently used PET-films were PET 505 and Mylar A (Dupont Teijin Films). PET 505 has a smoother surface than Mylar A. On the other hand, the transfer of polymeric solutions by coating techniques was improved by using Mylar A. Therefore, it was selected as plastic substrate for the coating experiments. The PET-films were carefully cleaned by de-ionized water (DI water), acetone and isopropanol prior to use.

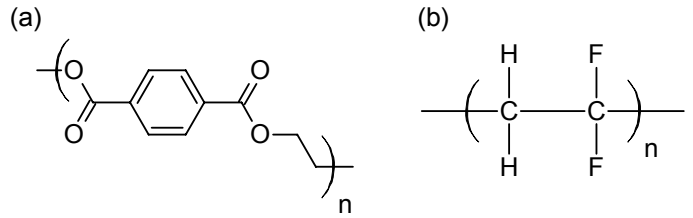

Chart 2.1. The chemical structures for (a) PET and (b) PVDF.

Unlike the HIFET, the substrate in the membrane based organic transistors (Papers 2, 3, 4 and 5) acts both as support and as electrolyte "insulator". A commonly used base-material for the membrane was the partly fluorinated poly(vinylidene fluoride) (PVDF) (Chart 2.1 b)). PVDF is known for its durability and chemical resistance and is therefore suitable for further manufacturing of devices. Because of the electrolyte within the membrane matrix, no extensive substrate-cleaning procedures were performed on the membranes. In Paper 3, however, the membranes were boiled in DI water before further processing in order to re-activate the hygroscopic electrolyte in the membrane and, hence, improve the ionic conductivity.

2.1.2 Contacts

A characteristic feature for the transistors in this thesis (with exception for Paper 3) is the use of conducting polymers for the gate electrode and metals (bulk and nanoparticle) for the source and drain electrodes. This is simply due to the different requirements set for the electrodes in the electrolyte gated OFETs as explained below.

In Section 1.2.3 it was discussed that, for an electrolyte gated OFET, the alignment of the gate relative to the active channel is not critical. Therefore, drop-casting of a conducting polymeric dispersion provides sufficient accuracy. Moreover, any risk of deteriorating the underlying polymeric layer can be avoided since drop-casting is a gentle method and the polymer does not require any heat treatment in order to become conducting. Therefore, the gate was applied by drop-casting a conducting polymeric dispersion in air (with exception for the all-printed HIFET in Paper 1). For drop-casting, either the water based PEDOT/PSS (Baytron P, H.C. Starck Gmbh) or the highly conducting salt of the emeraldine base-state of polyaniline (PANI) (Panipol T, Panipol Oy) were used. Chemical structures of the two conducting polymers are shown in Chart 2.2. For the all-printed HIFET, the gate was inkjetted in air with a Dimatix Materials Printer (DMP-2800, FUJIFILM Dimatix, Inc.). The inkjettable

and water based Baytron Jet PE FL and Baytron Jet HC (H.C. Starck Gmbh) PEDOT/PSS dispersions were used. The major concerns in selecting the proper conducting polymeric dispersions are the risk for dissolving or reacting with the underlying layer. Some of the used membranes, in Papers 2, 4 and 5, heavily reacts with the water based PEDOT/PSS, resulting in considerable swelling of the membrane matrix. In such cases the toluene based PANI (Panipol T) was a better choice.

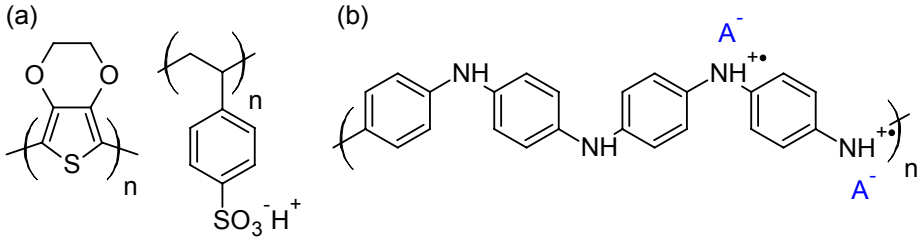

Chart 2.2. The chemical structures for (a) PEDOT/PSS and (b) the emeraldine salt form of PANI.

In order to maintain consistency of the electronic behavior between transistors, it is essential to carefully control the dimensions of the active channel (*L* and *W*). In this thesis, vacuum evaporation of gold through a shadow mask was used in order to yield the source and drain electrodes. Gold provides a nearly ohmic contact towards the used p-channel semiconductor. The contact resistance is further minimized by the high conductivity of metals. Vacuum evaporation also allows for the thickness of the structures to be controlled in a nanometer-scale resolution. For the all-printed HIFETs (Paper 1) the source and drain were inkjetted in air with DMP-2800. A silver nanoparticle dispersion (Cabot Corp.) was used for the purpose.

2.1.3 Semiconductors

Polymeric semiconductors benefit by being soluble (or dispersible) in common organic solvents and processable at low temperatures. Thus, they are attractive for roll-to-roll manufacturing purposes. In literature, a well-known polymeric semiconductor is the regioregular poly(3-hexylthiophene) (P3HT) (Chart 2.3) [43-45]. Because of the hexyl side-chains, the P3HT is soluble in common organic solvents. The hexyl side-chain is also short enough for good electronic transport. Moreover, by attaching the side-chains in a regioregular pattern, steric twisting of the polymer is reduced and the polymer self-organizes into a lamellar

structure [46-48]. For OFETs, the measured mobility and on/off ratio of well-ordered P3HT has been reported higher than 0.1 cm^2/Vs and 10^6 respectively [49-51], which are comparable to the inorganic a-Si MOSFETs.

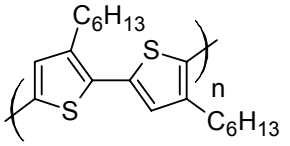

Chart 2.3. The chemical structure for the (regioregular) P3HT.

In this thesis, the P3HT semiconductor was used for all transistors (with exception for the all-polymer membrane based ECT in Paper 3). Two P3HT materials (Rieke Metals, Inc. and Plexcore, Inc.), supplied by Sigma-Aldrich Inc., was used. The P3HT was dissolved in either anhydrous chloroform (when spin-coated) or in a 1:1 mixture of toluene and p-xylene (when coated by reverse gravure). The P3HT was spin-coated, except for the all-printed HIFET in Paper 1. For the all-printed HIFET, the P3HT was applied in air by the reverse gravure coating technique. The reverse gravure coater was a tabletop Mini-Labo test coater (Yasui Seiki Co.).

For the membrane based ECTs in Paper 3, the redox-active polymer was PEDOT/PSS (Baytron P). It was printed by flexography using a Flexiproof 100 (R K Print Coat Instruments Ltd) flexographic printing unit.

2.1.4 Insulators

Polymeric dielectric insulators are soluble and often processable at low temperatures and, hence, suitable for plastic electronics. Moreover, unlike the frequently used SiO_2-insulator, all four transistor geometries can be employed (Figure 1.1). Polymeric insulators are, however, low-κ insulators and their break-down voltages are usually low. Therefore, and as discussed in Section 1.2.3, it has been popular to add a cross-linking agent in order to fabricate "sub-100 nanometer" robust polymeric insulators for low-voltage OFETs. On the other hand, the problem with substrate roughness becomes more significant. In Paper 1, a non-crosslinked poly(methyl methacrylate) (PMMA) (Sigma-Aldrich, Inc.) dielectric insulator was used for fabricating OFETs on different plastic substrates. The chemical structure is shown in Chart 2.4 a). The PMMA

was dissolved in ethylacetate and spin-coated onto the P3HT semiconductor.

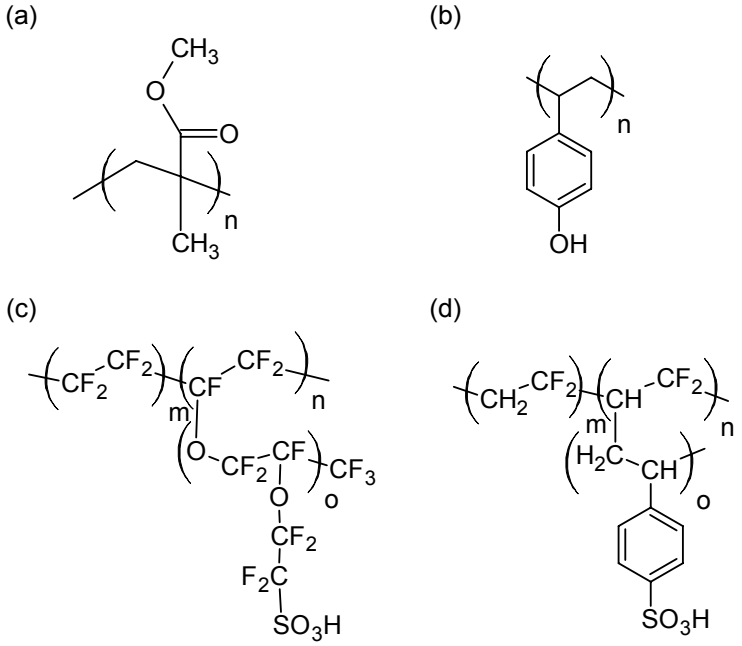

Chart 2.4. The chemical structures for (a) PMMA, (b) PVP, (c) PTFE:PFSA and (c) PVDF:PSSA.

The electrolyte "insulators", which were described in Section 1.2.3, are the central focus in this thesis. The ones used in this thesis are hygroscopic, that is, they require moisture to some extent for sufficient ionic drift. For the HIFETs in Paper 1, a hygroscopic poly(vinyl phenol) (PVP) was used (Chart 2.4 (b)). PVP is also a well-known polymeric dielectric insulator. In particular, by cross-linking the PVP the insulating properties are excellent [11, 18-20]. By exposing the non-crosslinked PVP to small protic solvents the PVP becomes proton conducting. The effect is utilized for operating the HIFETs at 1 V in air [26, 27]. In this thesis, the PVP (DuPont) was dissolved in isopropanol. It was either spin-coated or reverse gravure coated (for the all-printed HIFET) on the P3HT. The dry thickness of the PVP-insulator was between 1.0 - 1.5 µm.

All membranes in Papers 2, 3, 4, and 5 have a thickness between 50 - 150 µm. The two ion-conducting membranes that have received most attention in this thesis are tetrafluoroethylene-perfluoro-3,6-dioxa-4-methyl-7-octenesulfonic acid copolymer (PTFE:PFSA) and poly(vinylidene) poly(styrene sulfonic acid) (PVDF:PSSA) (Charts 2.4 (c) and (d)). PTFE:PFSA (trade name Nafion 115 (DuPont)) is a commercially

available fully fluorinated membrane that was purchased from ElectroChem Inc. It was used as received. The PVDF:PSSA (and the other ion-conducting membranes presented in Paper 2) was prepared by the electron beam irradiation induced grafting (EB) technique [52, 53]. The preparation of the PVDF:PSSA is illustrated in Scheme 2.1. Basically the EB technique consist of three major steps: (1) electron beam irradiation, (2) grafting, and (3) sulfonation (functionalization). The PVDF-base material was purchased from Goodfellow, Inc. and was washed with chloroform before irradiation.

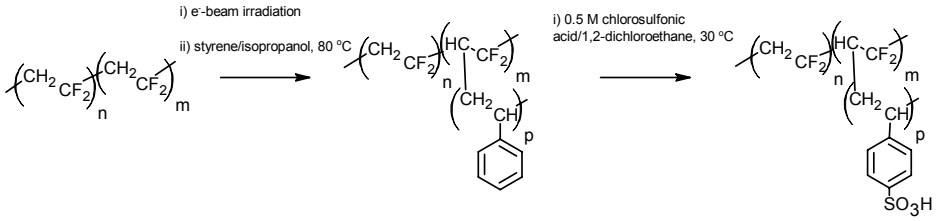

Scheme 2.1. The preparation scheme for the PVDF:PSSA. The three major steps are (1) irradiation, (2) grafting and (3) sulfonation (functionalization).

2.2 Measurements

2.2.1 Electrical Characterization

Most *I-V* and all current-time (*I-t*) analyses were done with an Agilent 4142B Parameter Analyzer (Agilent Tecnologies, Inc.) connected to a computer. While the OFETs, in Paper 1, were characterized in a nitrogen glovebox, the HIFETs were measured in air within a relative humidity (RH) interval of 25 – 35 %. In Paper 2 all MemFETs, except for the patterned PVDF:PSSA-based MemFET were measured in a nitrogen glovebox. The patterned MemFET was characterized in ambient air. In Paper 3, the *I-V* measurements were performed in a controlled humidity glovebox using a Keithley 2636 System Source Meter (source and drain) and a Keithley 2400 Source Meter (gate) (Keithley Instruments, Inc), both connected to a computer. While the PTFE:PFSA-based MemFETs, in Paper 4, were characterized both in a nitrogen glovebox and in RH = 5 – 10 %, they were solely measured in a nitrogen glovebox in Paper 5. All instruments were controlled with suitable LabView software (National Instruments Corp.).

In Paper 4, the *I-V* characterization of the PTFE:PFSA, at constant polarity (DC), was done both in ambient air and in a nitrogen glovebox. 25 nm thick gold electrodes were evaporated in vacuum, through a shadow mask. For the measurements through the membrane, the electrode area was set to 0.5 cm^2, while on the membrane the channel width was 1.0 cm and the channel length 1.0 mm.

For the impedance spectroscopy measurements in Paper 4, approximately 30 nm thick gold electrodes (surface area 0.5 cm^2) were evaporated in vacuum on both sides of the membrane. The sample was placed in an aluminum chamber and the chamber was vacuum pumped to a level of 10^{-3} – 10^{-4} mbar in which the measurements were done. The impedance spectroscopy measurements were carried out using a Gamry Reference 600 potentiostat (Gamry Instruments). The potentiostat was connected to a computer and controlled by suitable software. The AC amplitude was 15 mV and the frequency ranged from 1 MHz to 1 Hz with 10 points per decade. C_i was calculated from the obtained reactance values.

2.2.2 Optical Characterization

In Paper 5, the optical UV-Vis absorption analyses were performed in air with a Hitachi U-3200 Spectrophotometer (Hitachi High-Technologies Corp.) connected to a computer. The step length was set to 2 nm. During the thermal stress the samples were removed from the hotplate and allowed to cool down to room temperature prior to scanning.

In Paper 4, the optical transmission through the gold/PTFE:PFSA/P3HT/gold structures were measured in air. An incandescent tungsten lamp with a 435 nm cutoff filter was used as probe light. The light was focused on a 0.5 × 0.5 cm^2 area on the contact of the device, and the transmitted light was collected and focused into a SpectraPro 300i monochromator (Acton Research Corp.). The monochromated light was then measured using a Si-detector, a preamplifier and a SR830 lock-in amplifier (Stanford Research Systems, Inc.). The instruments were controlled with LabView software. For spectral measurements a wavelength range of 450 – 850 nm was used, and this range was scanned for applied voltages ranging from +2 V to -3V on the gate electrode. The voltage was applied for three minutes in order to allow the sample to reach equilibrium. In Paper 4, the transmission was monitored at the optical absorption region by continuously scanning from 540 nm to 550 nm with no pauses and simultaneously applying a sequence of voltages.

The atomic force microscopy (AFM) images in Paper 1 were scanned in ambient air and in non-contact mode with an AutoProbe CP (Park Scientific Instruments). All material preparation and experimental steps were handled in a nitrogen glovebox unless otherwise mentioned.

3. RESULTS AND DISCUSSIONS

This chapter is divided into five sections. Each section presents the main results and conclusions for respective paper that is covered in this thesis. The all-printed HIFET is presented in Section 3.1, with particular focus on the roughness of the used plastic substrate (Paper 1). The concept of utilizing ion-conducting membranes for manufacturing electrolyte gated OFETs (MemFETs) is demonstrated in Section 3.2 (Paper 2). In Section 3.3, the ion-conducting membranes are further introduced in all-polymer ECTs (Paper 3). Section 3.4 emphasizes the various deteriorating effects caused by the hydrous solid electrolytes on the OFET-behavior (Paper 4). Moreover, the idea of using sterically hindered phenolic antioxidants in order to inhibit device degradation is motivated in Section 3.5 (Paper 5).

3.1 Absence of Substrate Roughness Effects in Electrolyte Gated OFETs

The work evolved from the experiments on reverse gravure coating of both P3HT and PVP onto plastic substrates [54]. It was noted that a rougher plastic substrate (Mylar A, root mean square (RMS) roughness = 25 – 50 nm) was better suited than the smoother PET 505 (RMS roughness = 4 – 6 nm), for coating the second layer (PVP) without removing and deteriorating the first layer (P3HT). For a conventional OFET, an increased interfacial roughness will significantly alter the electronic transport in the active channel [51, 55-58]. However, for the all-printed HIFET, the *I-V* analysis did not reveal such defects albeit the active channel became rougher (Figure 3.1). Consequently, the target for this work was to point at the difference between the electrolyte gated OFET (HIFET) and the OFET when changing the plastic substrate from the smoother PET 505 to the rougher Mylar A. Additionally, a few possible explanations to the observed differences were discussed.

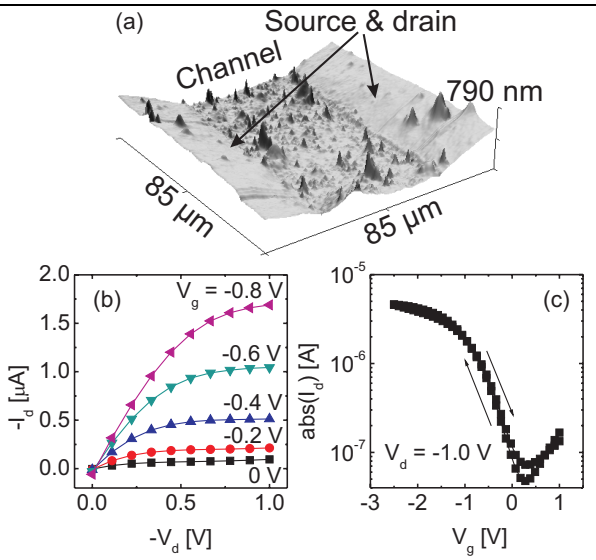

Figure 3.1. (a) The AFM picture illustrates the roughness of the active channel (after coating the Mylar A with P3HT) in the all-printed HIFET. The (b) output- and (c) transfer-characteristics of the all-printed HIFET. No pronounced deterioration due to increased roughness is observed.

A comparison between the OFET and the HIFET necessitates the fabrication of the devices by spin-coating and vacuum evaporation rather than using the coating and printing techniques. Hence, external uncertainties from, for example, impurities and variations in structural dimension are avoided. Therefore, the devices were manufactured by similar materials and methods and as much as possible in an inert atmosphere. A bottom-contact top-gate device structure was used for both the OFET and the HIFET (Figure 1.1 (d)). The fundamental difference, of course, was the use of the PMMA dielectric for the OFET and the hygroscopic PVP insulator for the HIFET. The thicknesses for respective insulator were estimated to 0.8 µm for the PMMA and 1.5 µm for the PVP. Eight OFETs and 14 HIFETs were studied for both substrates. The lower number of OFETs was enough to verify the effect of the rougher substrate, as previously observed in literature [56, 57]. Since the effect of the increased substrate roughness on the HIFET operation was particularly interesting in this study, a higher number of HIFETs were studied. Furthermore, a higher yield of HIFETs on both substrates simplified the statistical approach.

Transfer-curves for each device and on each substrate are shown in Figures 3.2 (c) and (d). All transfer-curves were measured in the saturated region. Additionally, the square-root of the drain currents are presented in Figures 3.2 (e) and (f). While the HIFET seems to be unaffected by the

increased roughness, the OFET displays expected deterioration, such as a lower on/off ratio, a lower subthreshold slope (S) and a decreased mobility. The change in mobility (μ) is interpreted from the slope (k) of the curves in Figures 3.2 (e) and (f). According to Equation (1.9), and when assuming that W, L, C_i and (V_G - V_T) are constant, the change in k is governed by the change in μ.

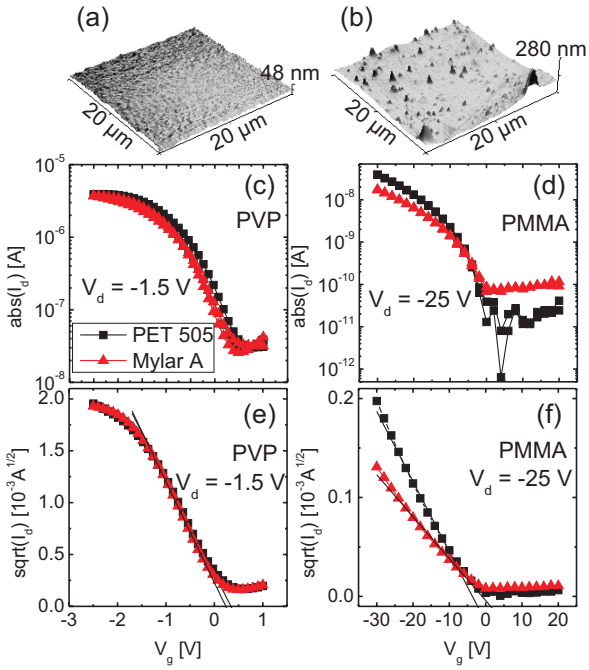

Figure 3.2. AFM pictures of (a) PET 505 and (b) Mylar A. Typical transfer-characteristics for (c) HIFETs and (d) OFETs manufactured on both substrates. The transfer-characteristics are measured in the saturated region. The square-root of I_{DS} for (e) HIFETs and (f) OFETs.

Table 3.1 summarizes the statistical results for both the OFET and the HIFET. These results support the observations made in Figure 3.2. Also the yields of functioning devices (i.e., devices that are comparable to the typical I-V curves in Figure 3.2) are shown. For the OFETs, the yield reflects the change in the substrate roughness. A higher RMS roughness increases the risk for electrical breakdown for the PMMA dielectric. The PVP is, however, almost twice the thickness of the PMMA. Moreover, the HIFET operates at substantially lower gate voltages. These two factors affect the higher yield of HIFETs on both substrates. The yield remains unaffected by the increasing substrate roughness. Another indicator, in favor for the HIFET, is the calculated standard errors. For the OFET, the

standard errors reveal larger fluctuations in quality between the OFETs, while the HIFETs show more consistency between each other.

Device	Substrate	On/off	*S* [V/decade]	*k* [$A^{1/2}$/V]	Yield [%]
HIFET	PET 505	10^2	0.80±0.05	$-(9.2\pm0.3)\times10^{-4}$	> 70
HIFET	Mylar® A	10^2	0.70±0.05	$-(9.1\pm0.3)\times10^{-4}$	> 70
OFET	PET 505	10^3-10^4	3.9±0.3	$-(7.4\pm1.2)\times10^{-6}$	~ 40
OFET	Mylar® A	10^2-10^3	7.0±0.8	$-(4.9\pm0.6)\times10^{-6}$	~ 20

Table 3.1. Average values of the on/off ratio, the subthreshold slope (S) and the slope of the square-root of I_{DS} (k) for all devices on respective substrate. The standard error has been calculated for S and k. Also the yields of functioning devices are shown.

Two arguments are pointed out to explain the higher stability in HIFETs. Firstly, it has earlier been shown that the HIFET is governed by the potential difference rather than by the electric field [27]. The ion migration at applied gate voltages causes the operation of the HIFET (as well as other electrolyte gated OFETs) to be independent to the insulator thickness. Thus, the thickness of the PVP layer does not alter the low-voltage behavior. Likewise, a similar smoothening effect could be possible at the rough semiconductor/insulator interface. Secondly, the higher capacitance that is gained by the hygroscopic PVP (as discussed in Section 1.2.3) generates more charges to the active channel to efficiently fill all the deeper trap states.

Besides the demonstrated all-printed HIFET on the Mylar A substrate [59], this work inspired to proceed towards even more challenging substrates, such as paper. Indeed, our group managed to demonstrate one of the first low-voltage polymeric transistors manufactured on a paper substrate [42]. After the publication of this work, other groups have independently also acknowledged the electrolyte gated OFET as being insensitive to an increased roughness [60, 61].

3.2 Self-Supported and Ion-Conducting Membranes for Low-Voltage Organic Transistors

Ion-conducting polymeric membranes (i.e., solid electrolytes) have been used in liquid and gas separation, fuel-cells and in the chlor-alkali industry. The thicknesses of the membranes are in the order of tens or hundreds of micrometers, which enables them to be self-supportive. By combining the bifunctional property of the membrane (the ion-conducting and self-supporting properties) with the electronic properties of the π-conjugated polymers, various and innovative organic electronic applications could be envisioned. The facility and know-how of preparing ion-conducting membranes were provided by the Laboratory of Polymer Technology. Therefore, the aim of this work was to present a concept of using ion-conducting membranes in organic electronics, and particularly, as a solid electrolyte "insulator" in OFETs (MemFETs).

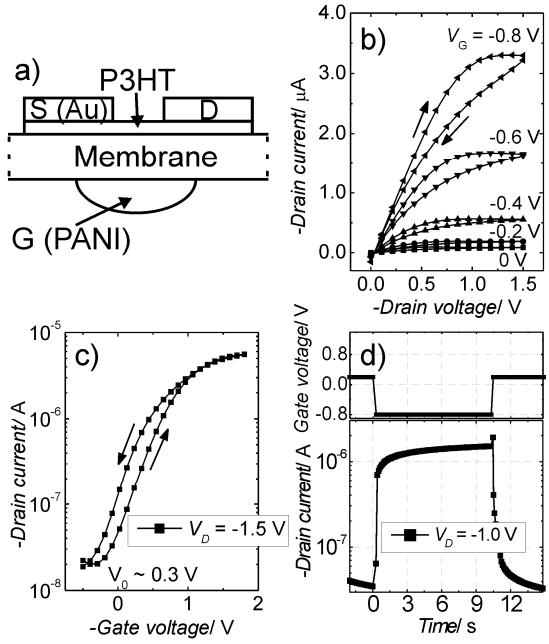

Figure 3.3. (a) The device structure for the MemFET. The (b) output- and (c) transfer-characteristics for the PTFE:PFSA-based MemFET. (d) The switch-on/switch-off response for the PTFE:PFSA-based MemFET.

The commercially available PTFE:PFSA (Nafion 115) is used as the "proof-of-concept" membrane (Figure 2.4 (c)). The membrane is transparent, has excellent mechanical properties and provides stable ionic conductivity at controlled atmospheres. Its morphology and ionic

transport properties have been thoroughly studied [62]. The hydrophobic fully fluorinated PTFE-backbone provides the support and the chemical resistance. In conjunction with the hydrophilic sulfonic acid groups the PTFE:PFSA self-organize to form hydrophilic nano-channels for ionic migration [63]. The self-organized morphology also results in a selective ionic transport. While protons migrate through the channels, anionic drift is prevented. The ionic conductivity is, furthermore, dependent on the water content in the membrane. Upon hydration, the channels swell and the ionic migration is improved, and vice versa upon drying.

The MemFET structure as well as the *I-V* and *I-t* characteristics for a PTFE:PFSA-based MemFET are shown in Figure 3.3. Apart from being a mechanical support, the membrane also acts as a platform for applying layers both on top and underneath the film. The characteristics are measured after one day of storing the devices in a dry atmosphere. The on/off ratio for the PTFE:PFSA-based MemFET is 10^2 – 10^3. The turn-on voltage (V_0) has a slight positive offset (0.3 V), much similar to the HIFET (see Section 3.1, Paper 1). Earlier reports suggest that P3HT is unintentionally doped by moisture in the insulator [27]. In Figure 3.3 (d), the switch-on reaches 65 % of the maximum on-current within one second. The switching time for the PTFE:PFSA-based MemFET can be faster by improving the ionic motion [64]. It will be shown in Section 3.4 (Paper 4) that the hydration level in the membrane largely affects the transistor-characteristics and presumably also the switching response. A hydrous PTFE:PFSA will improve the proton mobility and, hence, lower the polarization time.

For large-scale manufacturing purposes, the preparation of ion-conducting membranes by the EB technique provides a number of beneficial properties. The EB technique consists of three major steps (Scheme 2.1). Various polymeric base-materials can be used for electron beam irradiation. For all model membranes in Figure 3.4, the partially fluorinated PVDF was used, due to its similar properties compared to the PTFE. Additionally, the preparation of the PVDF is cheaper than the PTFE, which is a significant argument for large-scale manufacturing purposes. Sulfonic acid is the functional group (PVDF:PSSA) in Figure 3.4 (a), while, in Figure 3.4 (b), aminated vinylbenzyl chloride is grafted to the PVDF (PVDF:aminated VBC). In Figure 3.4 (c) the PVDF:PS is hosting a liquid lithium salt-solution of lithium hexafluorophosphate ($LiPF_6$) and aprotic solvents.

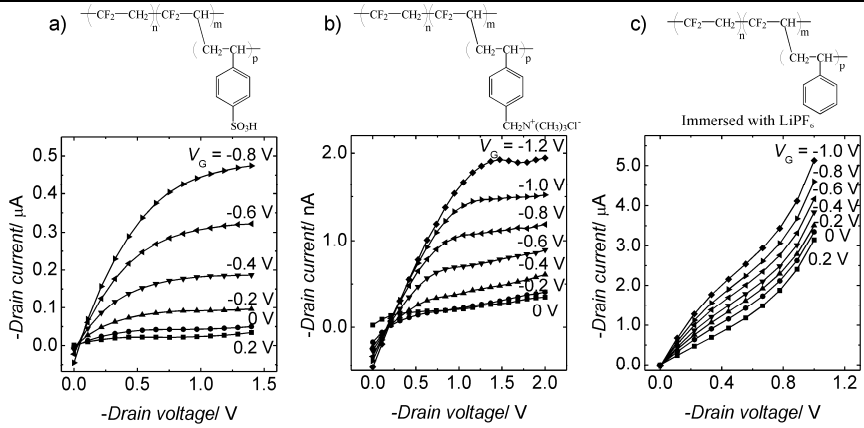

Figure 3.4. The chemical structures and the output-characteristics for MemFETs gated with (a) PVDF:PSSA, (b) PVDF:PS aminated VBC and (c) PVDF:PS immersed with a liquid solution of $LiPF_6$ and aprotic solvents.

The output-behavior for each model membrane differs drastically from each other which could reveal different doping conditions [65]. The different functional groups cause different ions to migrate in the membranes. The similarities between the output-curves of the PTFE:PFSA and the PVDF:PSSA is anticipated, since both membranes have the anions covalently bound to the polymeric backbone and are, thus, immobile. In Figures 3.3 (b) and 3.4 (a), I_{DS} is modulated by the electrostatic field-effect caused by the polyanionic EDL. On the other hand, both the PVDF:aminated VBC and the PVDF:PS immersed with a liquid solution of $LiPF_6$ and aprotic solvents contains mobile anions (Cl^- and PF_6^- respectively). Upon applying a negative V_G the anions migrate towards the membrane/P3HT interface. Depending on the bulkiness of the anion, the permeability of the P3HT and the applied V_G the degree of electrochemical doping the P3HT may vary [30, 65]. Unintentional electrochemical interaction of the P3HT is preferably avoided, since ionic drift into the polymeric semiconductor slows down the switch-on/switch-off of the device. Electrochemical bulk doping of the polymeric semiconductor may also result in a weakened saturation of I_{DS} or in a completely lost pinch-off. Moreover, the P3HT is structurally and electronically perturbed, which may lead to lower charge mobility, degrading performance and a reduced device lifetime. Some of these issues are further clarified in Section 3.4 (Paper 4). On the other hand, intentional electrochemical doping of the π-conjugated polymer can also be utilized for transistor-applications, as discussed in Section 1.2.3. The membrane-based ECT is demonstrated in Section 3.3 (Paper 3).

The key advantages for the ion-conducting membrane are the supporting structure and the ability to utilize the ionic transport for

several devices on the same membrane. For the latter, however, patterning of the electrolyte in the membrane would often be necessary in order to avoid unintentional crosstalk between neighboring devices. Furthermore, grafting of different functional groups on isolated parts of the same membrane could be envisioned for sensing purposes and for various devices. In the EB process, patterning is simply achieved by masking the base material during electron beam irradiation. Consequently, the grafting and the functionalization occur only at the unshielded (irradiated) parts of the base material. In this work, the PVDF was shielded by a patterned aluminum mask, to form PVDF:PSSA-dots (4 mm in diameter) separated by 10 mm from each other in a regular pattern (Figure 3.5). MemFETs were built both on top of the PVDF:PSSA-dots as well as on the unfunctionalized area to demonstrate the effect of patterning. It is noteworthy that, unlike the ordinary PVDF:PSSA-based MemFETs, it was possible to characterize the patterned MemFETs in air without any larger gate leakage currents caused by the ambient humidity. This can be explained by the restricted ion-conducting area, which prevents unconstrained diffusion of moisture in ambient air. Moreover, the PVDF:PSSA-dot is covered on both sides by the subsequent layers in the MemFET-structure.

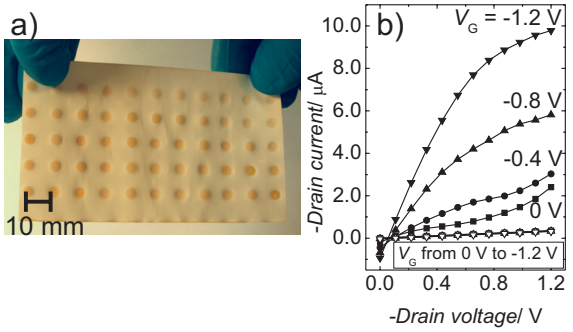

Figure 3.5. (a) The PVDF with ion-conducting PVDF:PSSA-dots in a regular pattern. (b) The MemFET on a PVDF:PSSA-dot (filled symbols) displays transistor behavior, whereas the MemFET on the bare PVDF only shows ohmic behavior (open symbols).

In this work, a MemFET and an electrochromic (EC) display pixel were fabricated on the same membrane (Figure 3.6) in order to demonstrate the ability of using the ionic properties for several and different organic electronic devices. Electrochromism is a well-known feature in π-conjugated polymers [66]. The reversible and the bias controlled color-switch usually follows two routes; either a switch between a colored and a bleached state or between two colored states. In the EC display pixel,

the electrolyte is used for inducing polaronic states by reversible redox-reactions and thereby achieving the switch in color. The emeraldine salt form of PANI is reversibly electrochromic when switching between the conducting (green) and the non-conducting state (blue). PANI was spin-coated onto the membrane to form the two electrodes that are separated by the ion-conducting membrane. The MemFET and the EC display pixel were connected with each other by silver paste. The switch from the steady-state to dark blue occurred within 30 s, which can be considered slow. The switching-time can be reduced, for example, by reducing the EC display pixel area (and thickness) and/or by improving the ionic conductivity and mobility. The latter argument, in particular, emphasizes the aforementioned possibilities that are enabled by the EB technique. For example, by patterning the membrane and by using different electrolytes for different devices, each device on the same membrane can be optimized for its own purpose.

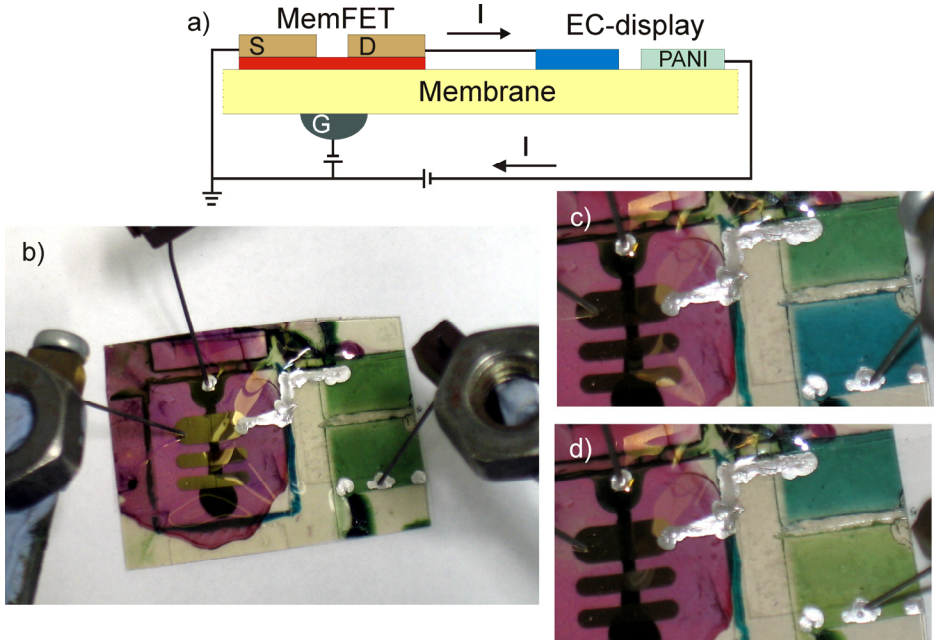

Figure 3.7. (a) The schematic structure of the MemFET + EC display pixel used in this work. (b), (c) and (d) The EC display pixel in action; (b) in the steady-state, (c) and (d) upon switching reversibly.

3.3 All-Polymer Low-Voltage ECTs on Patterned Ion-Conducting Membranes

Patterning of the membrane, as shown in Figure 3.5, is a simple and versatile method of controlling the ionic conductivity in the membrane. In this work, the technique was further elaborated and utilized for demonstrating all-polymer ECTs manufactured on patterned ion-conducting PVDF:PSSA membranes. The rather simple device structure and the low-voltage and stable operation that has been earlier demonstrated with the PEDOT/PSS based ECTs [38, 40, 41], attracts the ion-conducting membranes as suitable platforms for manufacturing ECTs by roll-to-roll manufacturing techniques.

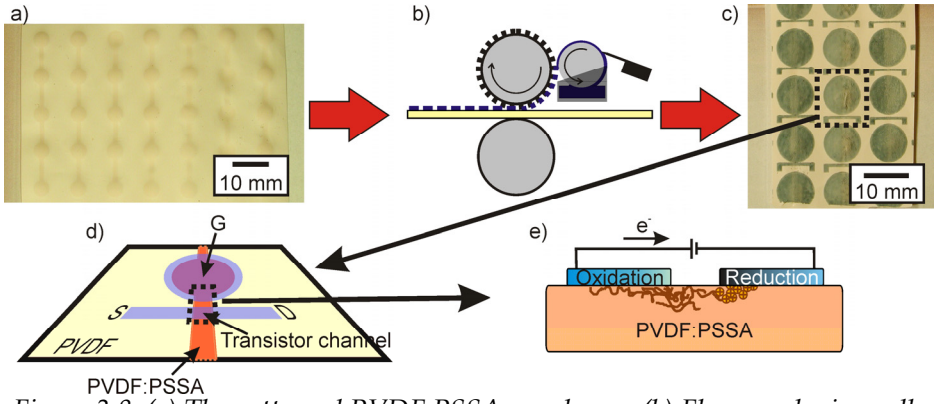

Figure 3.8. (a) The patterned PVDF:PSSA membrane. (b) Flexography is a roll-to-roll suitable printing technique. (c) A photograph of the printed ECTs on the patterned PVDF:PSSA membrane. (d) A schematic figure of the ECT structure. The source, drain and the gate are denoted by S, D and G respectively. (e) The transistor channel and the gate are coupled via the PVDF:PSSA. Thus they form an electrochemical cell, as schematically shown.

The membranes were prepared by the EB technique described in Scheme 2.1. Besides the PVDF:PSSA, the whole ECT structure consists of PEDOT/PSS, which is printed by flexography, as illustrated in Figure 3.8. Due to the redox-mechanism, the ECT can be fabricated in a lateral geometry, unlike OFETs. Therefore, all three electrodes can be placed on the same printing plate, and the device structure printed in one step. Naturally, this also reduces the issues related to electrode alignment. In this work, two modifications of the water-based PEDOT/PSS dispersion were done to improve the printed structure. Firstly, the viscosity of the dispersion was adjusted by partially removing water by evaporation. Hence, the resolution of the print pattern was improved. Additionally the

solid-content of the dispersion increased, which resulted in a higher conductivity. Secondly, ethylene glycol was added to the PEDOT/PSS dispersion. It is known that the addition of a high-boiling point polar solvent remarkably improves the conductivity in the PEDOT/PSS dispersion [67-70]. This is due to favorable morphological changes in the film formation that improves the charge percolation path.

A schematic view of the ECT is shown in Figure 3.8 (d). The electronic current between the source and drain is modulated by redox-reaction in the transistor channel. The transistor channel and the gate are coupled via the PVDF:PSSA and, thus, they form an electrochemical cell, as shown in Figure 3.8 (e). The reversible redox-mechanism for PEDOT/PSS is illustrated in Scheme 1.1. An increased reduction of PEDOT ($PEDOT^0$) in the transistor channel is obtained by applying an electric potential difference between the gate and the transistor channel (i.e., by addressing a positive gate voltage). Consequently, the electronic current through the transistor channel decreases. By removing the electric potential, the transistor channel is again oxidized, as described by Scheme 1.1. In this work, the transistor channel area was kept between 0.9 – 1.7 mm^2 while the gate electrode area was kept at 50 mm^2. Since there are more $PEDOT^+$- than $PEDOT^0$-sites in the PEDOT/PSS, the number of oxidation-sites in the gate is increased by increasing the gate electrode area [38, 40]. Thus, a higher on/off ratio is gained; in this work typically 10^2 – 10^3.

Three output-characteristics for a printed PEDOT/PSS based ECT are displayed in Figure 3.9. The characteristics are subsequently measured at delay-times (i.e., the time-gap between each voltage step) 1 s (open square), 5 s (filled circle) and finally at 1 s (open triangle) again. The lower current throughput at a higher delay-time corresponds to Equation (1.13). At longer delay-times a higher number of charges participate in reducing the transistor-channel. The minor mismatch between the first and the last characteristic (delay-time 1 s, open symbols) has not been clarified. It may stem from an incomplete oxidation of the transistor channel due to slow proton diffusion. But it may also be a small degradation of the PEDOT caused by an oxidative degradation in the presence of the hydrous electrolyte [71]. Oxidative degradation of P3HT (i.e., another polythiophene) in the hydrous MemFET setup will be further studied in Sections 3.4 and 3.5 (Papers 4 and 5).

The observed pinch-off of the current differs from the pinch-off mechanism for OFETs, as described in Section 1.2.2 [40]. The saturation of the current is caused by the reduction of PEDOT throughout the bulk of the transistor channel. At V_G = 0 V, and at higher $-V_{DS}$, protons are attracted into the transistor channel and gradually reduces the PEDOT closest to the PVDF:PSSA-interface.

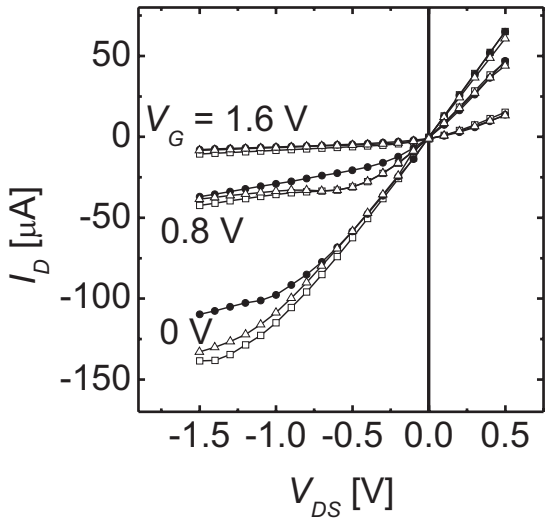

Figure 3.9. Output-characteristics for a PEDOT/PSS based ECT printed onto a patterned PVDF:PSSA membrane. The characteristics are subsequently measured at delay-times 1 s (open square), 5 s (filled circle) and 1 s (open triangle).

PEDOT/PSS is pristinely oxidized, as shown in Scheme 1.1. An overpotential will irreversibly overoxidize the polymer, which results in a dramatic loss of electronic conductivity [72]. Since overoxidation of PEDOT (and other polythiophenes) causes structural changes to the polymer and destroys the π-conjugation [71, 72], the loss in the electronic conductivity is permanent. This is shown in Figure 3.10, where a high oxidation potential (WRITE-pulse: V_G = -25 V, 5 s) decreases the current (I_{DS}) by several orders of magnitude. On the other hand, a high reduction potential (WRITE-pulse: V_G = 25 V, 5 s) does not deteriorate the conductivity in the transistor channel. The recovery seems to be almost complete already a few seconds after applying the WRITE-pulse. Thus, the ECTs are reversibly operated by reducing the transistor channel.

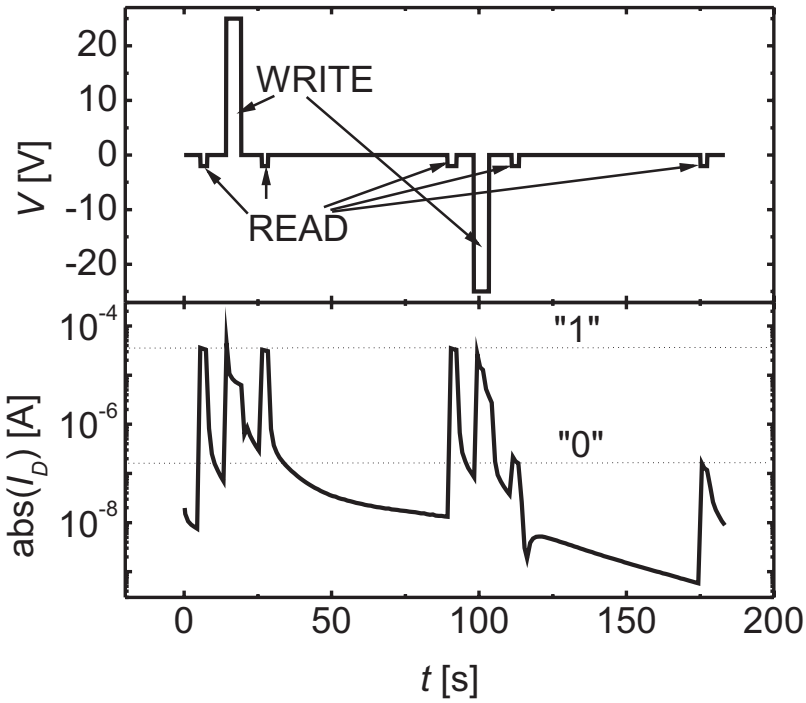

Figure 3.10. The figure illustrates the difference between applying a high reduction potential versus a high oxidation potential in a PEDOT/PSS based ECT. For the former the recovery of the current is almost complete, while the latter results in a terminated electronic conductivity. The WRITE-pulse is ±25 V, 5 s and the READ-pulse is -2 V, 2 s.

Overoxidation was utilized for demonstrating write-once read many times (WORM) memory functionality by using the ECT device structure (subsequently denoted as WORM-ECT). In a WORM-device, information is permanently stored once and read several times. Such memory-devices are considered favorable for e.g., archiving purposes. Organic WORM-devices have been demonstrated before [73-75]. *I-V* characteristics for the WORM-ECT are shown in Figure 3.11. By applying a high negative potential at the gate-electrode (WRITE-pulse: -25 V, 30 s) the transistor channel is overoxidized. In other words, the high-conducting state (“1”) is transformed into a low-conducting state (“0”). The permanent “0” state is further illustrated by characterizing the WORM-ECT roughly one month afterwards. From Figure 3.11 it is apparent that the “0” state is not completely stable. The variation in conductivity is due to the ionic conductivity in the WORM-ECT, which is sensitive to a change in the ambient humidity.

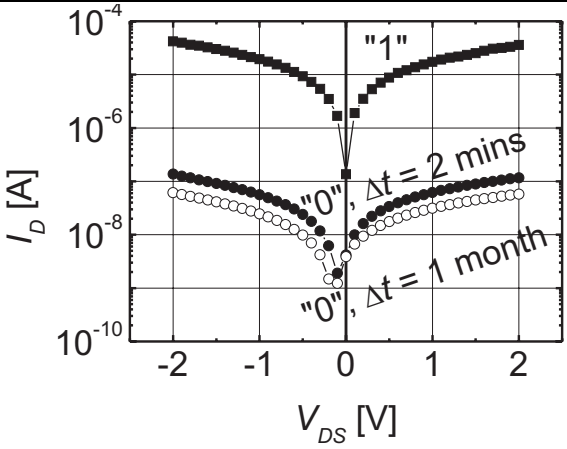

Figure 3.11. The WORM-ECT characterized before and after applying the WRITE-pulse. Minor deviations in the "0"-state occurs due to small variations in the ambient humidity.

It is noteworthy that the WRITE-period for the presented device is fairly long. This was intentionally chosen in order to ensure complete overoxidation of the transistor channel and, hence, demonstrate the WORM memory functionality. By optimizing the volume of the transistor channel and/or improving the ionic conductivity of the PVDF:PSSA, the WRITE-pulse could be shortened, which possibly would attract the WORM-ECT towards practical applications.

3.4 The Role of Moisture in Hydrous Electrolyte Gated OFETs

In the efforts of improving the performance of the sulfonic acid-based MemFETs (PTFE:PFSA and PVDF:PSSA), described in Section 3.2 (Paper 2), it was observed that moisture management and voltage control was highly crucial in order to avoid deteriorating effects. The latter, in particular, was somewhat surprising since the maximum electric potential that could be applied was reached already below 1.5 V. Furthermore, one of the main arguments for using membranes for (p-channel) electrolyte gated OFETs was to avoid electrochemical interaction (See Sections 1.2.3 and 3.2) Moisture was at an early stage assumed to be the root cause for the observed deterioration. Therefore, the effects from moisture in hydrous electrolyte gated OFETs were clarified in this work. The work is divided in two parts: the first part deals with the reversible

deterioration and the second part presents the irreversible degrading effects caused by the presence of moisture.

3.4.1 The Effects of a Varying Ambient Humidity

In this work, PTFE:PFSA (Nafion 115) was selected as the model membrane, mainly because of its optical transparency. The PTFE:PFSA membrane is commercially available and was used as received.

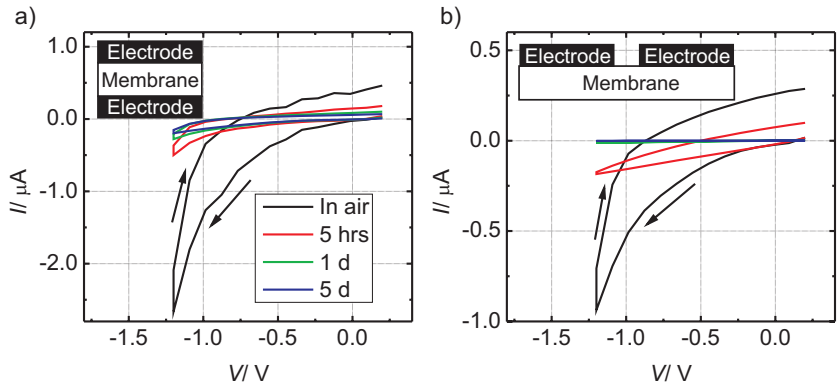

Figure 3.12. Characterization at constant polarity (a) through the PTFE:PFSA, and (b) on the surface of the membrane. The measurements were done in ambient air and as a function of time in a dry atmosphere.

In Figure 3.12, *I-V* characteristics are swept at constant polarity both through the PTFE:PFSA (Figure 3.12 (a)) and on the surface of the membrane (Figure 3.12 (b)). In ambient air both measurements display similar behavior. At a small negative offset, there already is a strong non-linear increase in the current in the forward sweep (from 0.2 V to -1.2 V). The non-linear trend diminishes when exposing the samples to a dry atmosphere. The non-linear characteristic is a clear evidence for the water electrolysis current (i.e., Faradaic current) [76], which obviously looses significance upon drying the membrane. From Figure 3.12 it is also clear, that the surface of the PTFE:PFSA dries fast (Figure 3.12 (b)) compared to bulk (Figure 3.12 (a)). The *I-V* behavior, in Figure 3.12 (b), is completely linear after five days of storing the sample in a dry atmosphere, intersects at origo and has dropped by several orders of magnitude. Thus, the remaining current mainly constitutes of a small charging current and electronic leakage. It is noteworthy that the electrical stress and the resulting water electrolysis that the samples are subjected to (in a dry

atmosphere) accelerate the drying of the membrane. Moisture in the membrane is simply consumed faster when a voltage is applied over it.

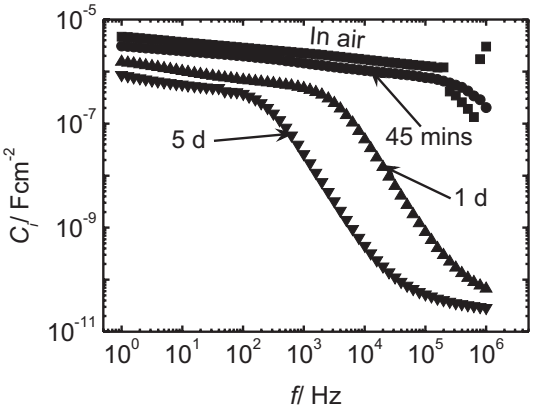

Figure 3.13. The C_i was calculated at different frequencies from the impedance spectroscopy measurements. The measurements were done in ambient air and as a function of time in vacuum.

Impedance spectroscopy was used to characterize C_i as a function of the AC frequency, as shown in Figure 3.13. The AC amplitude was 15 mV and the frequency was scanned at zero offset bias, in order to minimize the effect from water electrolysis. In Figure 3.13, C_i is monitored in air and as a function of time in vacuum. The maximum C_i, measured at low frequencies and in ambient air, is 5 μF/cm². The capacitance-value is typically 2 – 10 times lower than usually found for electrolytes [28, 29, 31, 32, 64], which corresponds to the discussion in Sections 1.2.3 and 3.2. Since the polyanion is covalently bound to the base-polymer it will be virtually immobile. The total C_i over the electrolyte will therefore be lower and the electric field distribution will be broadly distributed at the membrane/P3HT interface, as schematically illustrated in Figure 1.4 (c). On the other hand, we anticipate that the immobile polyanion is hindered from penetrating and electrochemically interacting with the polymeric semiconductor.

In Figure 3.13, it is clear that both the characteristics and C_i changes with time in vacuum. Firstly, the C_i at lower frequencies continuously drops with time in vacuum. Secondly, the C_i becomes strongly frequency dependent in vacuum and the "knee" shifts towards lower frequencies with longer time in vacuum. Both features correspond to the gradual drying of the PTFE:PFSA. The hydrophilic nano-channels in the PTFE:PFSA (described in Section 3.2) shrink [62, 63], starting from the surfaces of the membrane, which results in a poor ionic re-orientation and, hence, in a lower C_i. Furthermore, the ions become unable to

completely re-orient themselves at higher frequencies. Apparently, the ionic mobility drops.

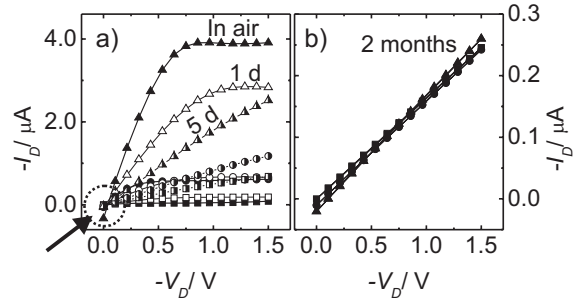

Figure 3.14. (a) Typical output-characteristics measured for a PTFE:PFSA-based MemFET in ambient air and as a function of time in a dry atmosphere. The arrow points at the gate leakage current caused by the hydrous electrolyte. The gate leakage current diminishes upon drying the membrane. (b) Output-characteristics for a PTFE:PFSA-based MemFET measured after two months of storing in a dry atmosphere. The applied V_G´s are 0 V (square), -0.4 V (circle) and -0.8 V (triangle).

Based on the aforementioned observations on the bare PTFE:PFSA, a changing ambient humidity should also have a detrimental impact on the charge transport in the MemFET. Indeed, as seen in Figure 3.14, the output-curves loose their transistor-characteristic features (i.e., the pinch-off and the modulation) by keeping the PTFE:PFSA-based MemFET in a dry atmosphere for two months. If assuming that W, L and $(V_G - V_T)$ are constant, throughout the measurements in Figure 3.14, then the observed decrease of the channel conductance (g_D) at $V_{DS} << V_G$ is caused by μC_i, according to Equation (1.3). This is verified by the decreasing C_i in Figure 3.13. Consequently, and unlike OFETs, C_i is a considerable variable and the drying of the membrane is symptomatic of the transition of the hydrous electrolyte gated OFET towards a poorly performing low-voltage OFET with a 100 µm thick dielectric insulator. It should be noted that the effects from the varying ambient humidity are reversible. By hydrating the dried PTFE:PFSA the output-characteristics are restored. However, at RH > 10 %, the PTFE:PFSA-based MemFET suffers from an increasing ionic conductivity [76]. Therefore, careful balancing of the ambient humidity levels is essential on a longer time-scale.

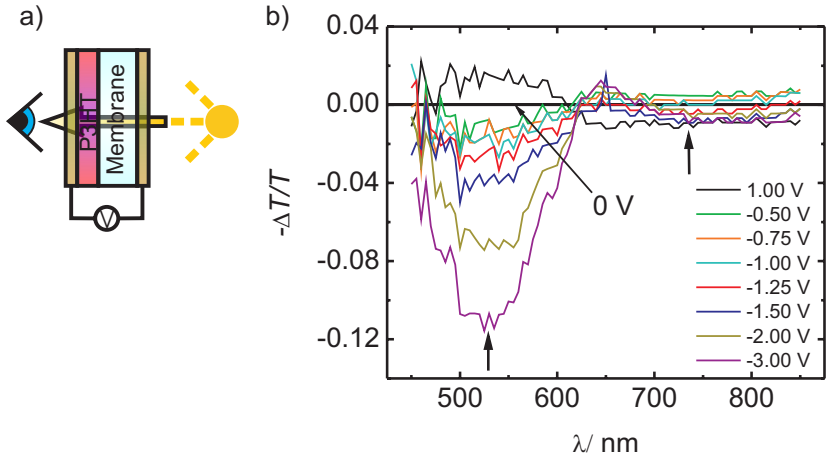

Figure 3.15. (a) A schematic illustration of the experimental setup for the optical studies. (b) The change in transmission was characterized for the P3HT/PTFE:PFSA sample in air at different voltages applied on the gate. The π-π absorption region and the polaron absorption regions are indicated by the arrows.*

3.4.2 Irreversible Degradation at Higher Electric Potentials

Electronical and structural changes in the polymeric semiconductor can be monitored *in situ* by registering the changes in the optical transmission spectrum at different voltage steps [30]. In this work, the change in transmission was studied in an experimental setup as schematically shown in Figure 3.15 (a) (the experimental details are described in Section 2.2.2). The sample resembles the MemFET-structure and the voltages are applied on the gate electrode. The obtained spectra are plotted in Figure 3.15 (b). Two regions of interest are indicated by the arrows. Firstly, the π-π* absorption region for P3HT is at 500 – 550 nm, which is the specific bandgap energy for the polymeric semiconductor. Secondly, the polaron absorption region is at > 700 nm. Three specific regions are identified in Figure 3.15 (b). Firstly, at V_G = +1 V, the P3HT is depleted from charges, which is manifested as an increased absorption ($-\Delta T/T > 0$) in the π-π* region and a photobleaching ($-\Delta T/T < 0$) in the polaron region. Secondly, at -1.25 V < V_G < 0 V the P3HT is doped, which is seen as a small photobleaching in the π-π* region and an increased absorption in the polaron region. Correspondingly, delocalized charges are induced in the P3HT. Thirdly, at V_G < -1.25 V photobleaching occurs in both regions. Because of the dramatic photobleaching in the π-π* region (particularly below -1.5 V) there is a perturbation on the molecular level of the P3HT.

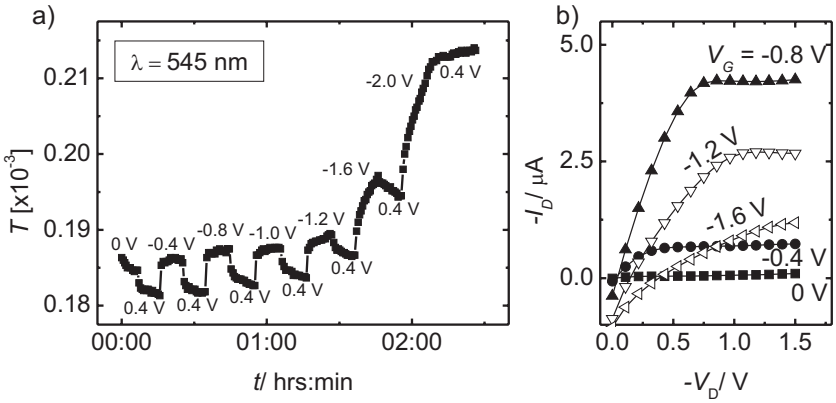

Figure 3.16. (a) The optical transmission recorded in the π-π absorption region for the P3HT/PTFE:PFSA sample in air. The transmission is monitored at different gate voltage steps. The experimental setup is shown in Figure 3.15 (a). (b) Output-characteristics for a PTFE:PFSA-based MemFET in air.*

In Figure 3.16 (a) the transmission (T) in the π-π* region is studied by applying a sequence of voltage steps. The system is dedoped by a positive bias of 0.4 V, according to the off-state of the PTFE:PFSA-based MemFET (Figure 3.3 (c)). The optical behavior is further compared to the typical output-characteristic measured for a PTFE:PFSA-based MemFET (Figure 3.16 (b)). Both measurements are done in air. However, the MemFET characterization is performed in a slightly drier air (RH = 9 – 10 %), compared to the optical characterizations (RH = 25 – 30 %), in order to diminish the influence from gate leakage currents. The observed trend in Figure 3.15 is also seen in Figure 3.16. At -1.2 V < V_G < 0 V, the change in T is small, relatively fast and reversible. Furthermore, T remains constant upon applying the doping-bias and the change is nearly equal for all the bias steps within the interval. All these facts correspond to the electrostatic doping of the P3HT, which is verified by the OFET-characteristic curves (Figure 3.16 (b)) within the same interval. On the other hand, at V_G < -1.2 V, the change in T becomes large, continuously growing and irreversible. In the output-characteristic this is identified as a clear deterioration of the modulation and the pinch-off. The system has evidently entered a regime of irreversible degradation.

The observed degradation in Figures 3.15 and 3.16 can be further distinguished by studying a sequence of several transfer-sweeps characterized in a dry atmosphere. Figure 3.17 displays 25 consecutively measured transfer-sweeps for PTFE:PFSA-based MemFETs. In Figure 3.17 (a) the transfer-measurements are carried out in the saturated region, while they are characterized in the linear region in Figure 3.17 (b).

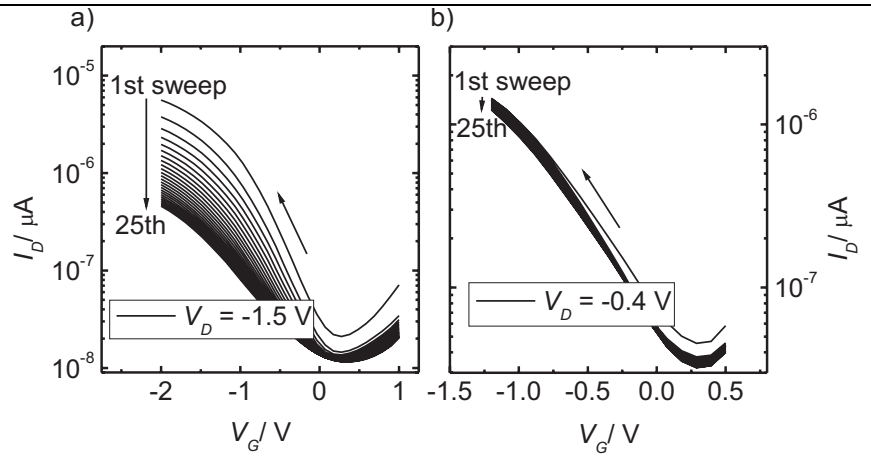

Figure 3.17. 25 consecutive forward scans for PTFE:PFSA-based MemFETs measured (a) in the saturated region, and (b) in the linear region.

Moreover, in Figure 3.17 (b), the electric potential never exceeds 1.2 V between any two electrodes. Based on the results it can be concluded that the onset for the degradation of the transfer-curve, in Figure 3.17 (a), is bias-dependent. These results correspond with the aforementioned observations in Figures 3.15 and 3.16.

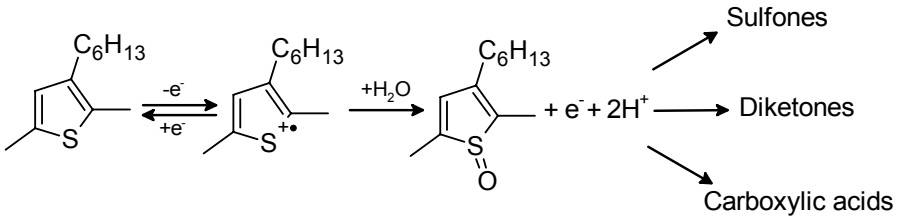

Scheme 3.1. The obtained results in Section 3.4.2 support the following reaction mechanism. Reversible doping of the P3HT occurs at -1.2 V < V_G < 0 V for the PTFE:PFSA-based MemFET. At V_G < -1.2 V, oxidative degradation of the P3HT will be initiated by significant water electrolysis in the hydrous electrolyte. The sulfoxide group will further react and the semiconducting properties of the P3HT will be lost.

The experimental results obtained in this work point towards the degradation of polythiophenes by oxidation, which is initiated by water electrolysis in the hydrous electrolyte (Scheme 3.1). For the PTFE:PFSA-based MemFET the onset for severe oxidative degradation is at $V_G \approx$ -1.2 V. (Over)oxidative degradation of polythiophene-derivatives has been studied before [71, 72, 77-79]. For example, according to Barsch, et. al. [71], the complete degradation mechanism consists of several steps that

will result in chain breaking and in the loss of conjugation. In other words, the conducting pathway will be disrupted.

3.5 Improved Device Stability by Adding a Sterically Hindered Phenolic Antioxidant in P3HT

In Section 3.4 (Paper 4) it was shown that the P3HT is susceptible to degradation by oxidation at electric overpotentials in a hydrous electrolyte gated OFET. This will, of course, have detrimental consequences for the long-term stability of the transistor. There are three alternatives for reducing the degradation: (1) by choosing a less hygroscopic electrolyte. For example, the HIFET can be operated at a broader electric potential interval and at higher RH levels than the PTFE:PFSA-based MemFET. (2) By controlling the electric potential interval. This was shown in Figure 3.17. (3) By protecting the polymeric semiconductor from oxidative degradation with a sterically hindered phenolic antioxidant. This is a well known method for inhibiting polymeric decomposition of conventional polyolefins [80]. In this section it will be demonstrated that sterically hindered phenolic antioxidants can also be used for improving the stability of π-conjugated polymers.

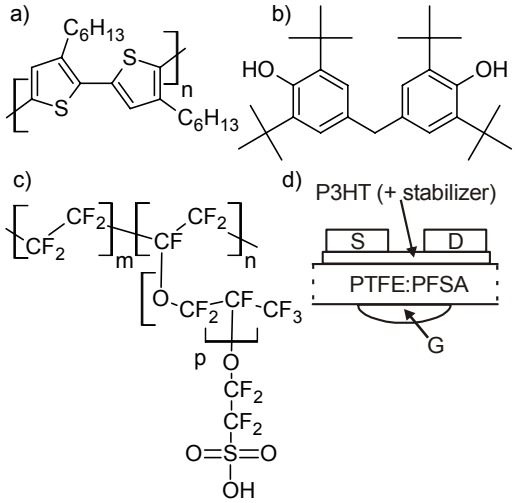

Figure 3.18. The chemical structures of (a) the P3HT-semiconductor, (b) the 4,4´-methylenebis(2,6-di-tert-butyl phenol)-stabilizer, and (c) the PTFE:PFSA-membrane. (d) The structure for the MemFET.

The PTFE:PFSA-based MemFET is used as the model device (Figure 3.18). The sterically hindered phenolic antioxidant 4,4´-methylenebis(2,6-di-tert-butyl phenol) (subsequently denoted as stabilizer) is added into the P3HT-solution. The chemical structure for the stabilizer is shown in Figure 3.18 (b) and the stabilization mechanism is illustrated in Scheme 3.2. Accordingly, the stabilizer structure serves several purposes [80]. Highly reactive alkoxy and peroxy radicals are stabilized by the easily abstractable hydrogen from the phenolic moiety. Furthermore, the antioxidant complex is stabilized by the resonance structure, provided by the aromatic system. The alkyl substituents at 2,6-positions provide two functionalities. Firstly, they enhance the hydrogen donating ability of the antioxidant. Secondly, they hinder the formed phenoxyl radical to further react by abstracting hydrogen from the polymeric backbone.

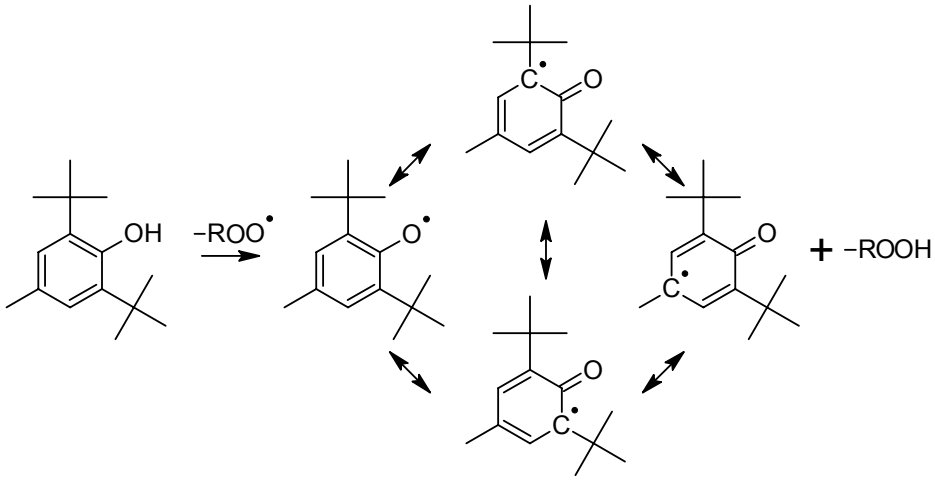

Scheme 3.2. The stabilization mechanism for sterically hindered phenolic antioxidants.

P3HT- and P3HT+stabilizer-samples were fabricated by spin-coating the solutions on respective glass substrates. Thermal stress studies were carried out in ambient air and in darkness at 110 °C. The change in the UV-Vis absorption was regularly monitored on the samples in order to observe any signs for improved lifetime in the stabilized P3HT. The results are depicted in Figure 3.19. The change in absorbance is similar in both cases. Initially, the annealing of the samples will improve the absorption but after a few hours of annealing both samples display bleaching of the absorbance peak. Further thermal stress will result in blue-shift of the peak and eventually to a complete loss of the absorbance [81]. Even though the bleaching seemingly falls with equal rates, after four hours of annealing, the absorbance is consistently higher throughout

the annealing process. Apparently, the stabilization occurs within the first few hours of annealing, which is verified by Figure 3.19 (b). Two features are distinguished in the stabilized P3HT. Firstly, the change in absorbance is relatively higher and, secondly, the improved absorbance occurs within two hours of annealing whereas the absorbance for the unstabilized P3HT decreases already after 30 minutes of annealing.

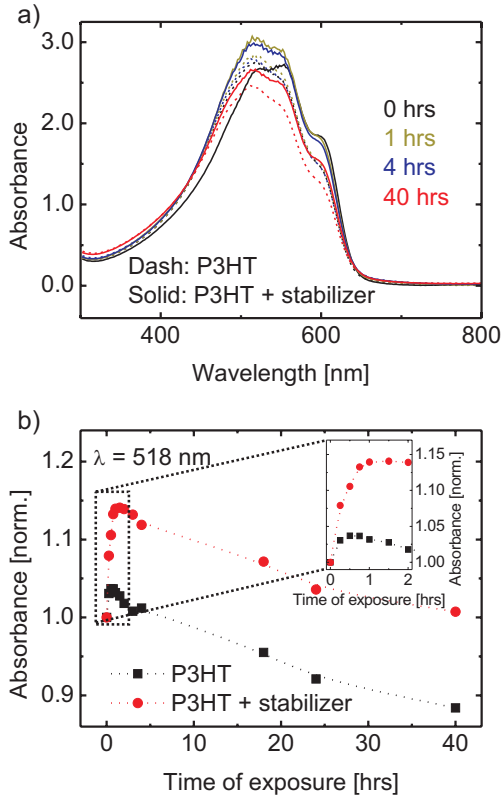

Figure 3.19. (a) UV-Vis absorption spectra of stabilized and unstabilized P3HT-samples upon annealing at 110 °C in air. (b) The normalized change in absorbance at 518 nm and as a function of time of annealing. The inset shows the change in absorbance for the first two hours.

The results in Figure 3.19 support that two major effects contribute to the changes in the absorbance: (1) densification of the P3HT-lattices [51, 82], and (2) thermooxidation of the P3HT [81]. The former characterizes the initial rise in the absorbance while the latter dominates at long-term annealing in air. Hence, in the stabilized P3HT, the polymer is initially protected from thermooxidation by the sterically hindered phenolic antioxidant. Eventually, however, the stabilizer will be consumed and the

thermooxidation will continue with the same rate compared to the unstabilized P3HT.

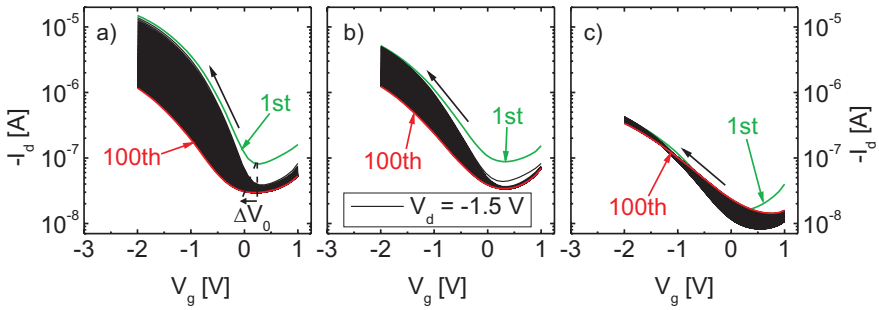

Figure 3.20. 100 consecutive transfer-characteristics measured in the saturated region for (a) an unstabilized MemFET and for MemFETs having a stabilizer concentration of (b) 500 ppm by weight and (c) 1:1 by weight. Only the forward sweeps are shown. The first (green) and the 100th sweep (red) are also indicated.

The used stabilizer concentration in the UV-Vis analysis is 1:1 by weight (relative to the P3HT). From the observations in Figure 3.19 it is anticipated that even higher concentrations would further improve the lifetime of the P3HT. However, such concentrations of an "impurity" will naturally affect the charge transport in the P3HT in an unfavorable fashion. In Figure 3.20, 100 consecutive transfer-sweeps, measured in the saturated region, are shown for an unstabilized MemFET (3.20 (a)) and for MemFETs having a stabilizer concentration of 500 ppm by weight (3.20 (b)) and 1:1 by weight (3.20 (c)). Clearly, adding the stabilizer decreases the pristine on-current. Furthermore, by calculating μ, according to Equation (1.10) (assuming that W, L and C_i are identical for the devices), the difference between the first sweeps in Figures 3.20 (a) and (c) is two orders of magnitude. Nevertheless, the fall of the on-state throughout the 100 sweeps is at its minimum in Figure 3.20 (c). In other words, the stabilizer protects the P3HT from oxidative degradation that would be caused by the applied electric overpotentials, as described in Section 3.4 (Paper 4). Furthermore, Figure 3.20 (b) demonstrates that the negative effects on the electronic performance can be reduced by lowering the stabilizer concentration without loosing the stabilizing effect.

In Scheme 3.2 it was shown that oxidative degradation of the P3HT results in a disrupted charge percolation. This would imply that a higher electric potential is required in order to accumulate mobile charges and establish the active channel between the source and drain. A higher negative shift of V_0 is indeed distinguished for the unstabilized MemFET (see Figure 3.20). Correspondingly, when estimating V_T from Equation

(1.4) a similar trend was also observed. However, the analysis provided somewhat contradictory results, which is ascribed to the decaying C_i throughout the 100 transfer-sweeps. Water electrolysis occurs at higher voltages and since the devices are measured in a dry atmosphere the moisture will eventually be depleted. With prolonged scans the ionic polarization in the membrane is deteriorated, which, according to Equation (1.4), affects the slope and the on-current in the transfer-characteristics. It should be emphasized that this effect should be identical for all MemFETs in Figure 3.20. Noteworthy is that, for the stabilized MemFET in Figure 3.20 (c), V_0 shifts towards positive voltages after roughly 30 transfer-sweeps. The effect is probably caused by the increasing concentration of phenoxyl radicals, in the P3HT, acting as unintentional dopants. The effect is not visible in Figure 3.20 (b).

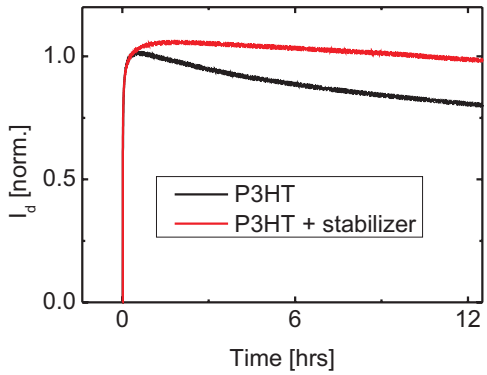

Figure 3.21. The normalized I_{DS} as a function of time with constant applied V_{DS} = -1.5 V and V_G = -1.0 V.

The problems associated to a decaying C_i can be avoided by applying a constant V_{DS} and V_G. Thus, a high charge density is continuously concentrated in the active channel. In Figure 3.21, the *I-t* characteristics are monitored in the on-state for an unstabilized and a stabilized MemFET. Accordingly, the on-current decreases more rapidly in the unstabilized device, compared to the stabilized MemFET, which corresponds to the oxidative degradation of P3HT. Such degradation is not observed for the stabilized MemFET and the obtained results in Figure 3.21 are yet another evidence for the protective effect of the sterically hindered phenolic antioxidants against P3HT degradation.

4. SUMMARY

The reported results in this thesis have broadened our knowledge concerning ion modulated organic transistors and resulted in new ideas towards printed organic electronics. The previous work on the HIFET-concept, conducted in our laboratory, was used as the starting-point. By directly comparing ordinary OFETs with HIFETs we have been able to show that the HIFET (as well as other electrolyte gated OFETs) are less sensitive to an increased roughness of the substrate. Consequently, all-printed and low-voltage HIFETs have been demonstrated on both plastic and paper substrates.

We have also demonstrated ion modulated organic transistors built on ion-conducting membranes (solid electrolytes). The membrane functions as a platform for fabricating the devices. Moreover, by using the EB technique, the membranes can be functionalized and tailor-made in any desired fashion.

The role of water in hydrous electrolytes has been clarified. Firstly, unlike traditional OFETs, the capacitance should often be considered as a variable because of the varying humidity level in the hydrous electrolyte "insulator". Secondly, moisture has both a reversible and an irreversible deteriorating effect on the device behavior. The former can be largely handled by controlling the ambient humidity. The latter degradation, on the other hand, can be diminished by using a less hygroscopic electrolyte and/or by carefully controlling the electric potentials in the device. Alternatively, we have shown that the degradation can be quenched by adding a sterically hindered phenolic antioxidant into the polymeric semiconductor.

In future research, improved consistency and device stability should be emphasized. These key-issues could be more essential for printed applications than e.g., the efforts towards "state-of-the-art" charge mobilities or on/off ratios. In this thesis, the ion-conducting membranes have been mainly associated with ion modulated organic transistors. In future, the concept will be further broadened. For example, various sensing applications might enable new possibilities for research. The ion modulated organic transistor could be built on the same membrane and utilized e.g., as a signal amplifier. Thus, the multifunctional properties of the membranes and the ion-to-electron transducing opportunities would be brought up to new levels.

BIBLIOGRAPHY

[1] J. Bardeen, W. H. Brattain. The Transistor, a Semi-Conductor Triode. *Phys Rev.* **74**, 230-231 (1948).

[2] D. Kahng. Electric Field Controlled Semiconductor Device. US Patent 3 102 230 (1963).

[3] C. K. Chiang, C. R. Fincher, Y. W. Park, A. J. Heeger, H. Shirakawa, E. J. Louis, S. C. Gau, A. G. MacDiarmid. Electrical Conductivity in Doped Polyacetylene. *Phys. Rev. Lett.* **39**, 1098-1101 (1977).

[4] H. S. White, G. P. Kittlesen, M. S. Wrighton. Chemical Derivatization of an Array of Three Gold Microelectrodes with Polypyrrole: Fabrication of a Molecule-Based Transistor. *J. Am. Chem. Soc.* **106**, 5375-5377 (1984).

[5] A. Tsumura, H. Koezuka, T. Ando. Macromolecular electronic device: Field-effect transistor with a polythiophene thin film. *Appl. Phys. Lett.* **49**, 1210-1212 (1986).

[6] M. Berggren, A. Richter-Dahlfors. Organic Bioelectronics. *Adv. Mater.* **19**, 3201-3213 (2007).

[7] R. A. Street, A. Salleo. Contact effects in polymer transistors. *Appl. Phys. Lett.* **81**, 2887-2889 (2002).

[8] Y. Roichman, N. Tessler. Structures of polymer field-effect transistor: Experimental and numerical analyses. *Appl. Phys. Lett.* **80**, 151-153 (2002).

[9] T. J. Richards, H. Sirringhaus. Analysis of the contact resistance in staggered, top-gate organic field-effect transistors. *J. Appl. Phys.* **102**, 094510 (2007).

[10] L.-L. Chua, P. K. H. Ho, H. Sirringhaus, R. H. Friend. High-stability ultrathin spin-on benzocyclobutene gate dielectric for polymer field-effect transistors. *Appl. Phys. Lett.* **84**, 3400-3402 (2004).

[11] Y.-Y. Noh, N. Zhao, M. Caironi, H. Sirringhaus. Downscaling of self-aligned, all-printed polymer thin-film transistors. *Nat. Nanotechnol.* **2**, 784-789 (2007).

[12] L. Burgi, R. Pfeiffer, C. Winnewisser. Submicrometer polymer transistors fabricated by a mask-free photolithographic self-alignment process. *Appl. Phys. Lett.* **92**, 153302 (2008).

[13] J. N. Haddock, X. Zhang, S. Zheng, Q. Zhang, S. R. Marder, B. Kippelen. A comprehensive study of short channel effects in organic field-effect transistors. *Org. Electron.* **7**, 45-54 (2006).

[14] C. Tanase, E. J. Meijer, P. W. M. Blom, D. M. de Leeuw. Unification of the Hole Transport in Polymeric Field-Effect Transistors and Light-Emitting Diodes. *Phys. Rev. Lett.* **91**, 216601 (2003).

[15] C. D. Dimitrakopoulos, S. Purushothaman, J. Kymissis, A. Callegari, J. M. Shaw. Low-Voltage Organic Transistors on Plastic Comprising High-Dielectric Constant Gate Insulators. *Science* **283**, 822-824 (1999).

[16] C. Bartic, H. Jansen, A. Campitelli, S. Borghs. Ta_2O_5 as gate dielectric material for low-voltage organic thin-film transistors. *Org. Electron.* **3**, 65-72 (2002).

[17] G. Wang, D. Moses, A. J. Heeger, H.-M. Zhang, M. Narasimhan, R. E. Demaray. Poly(3-hexylthiophene) field-effect transistors with high dielectric constant gate insulator. *J. Appl. Phys.* **95**, 316- (2004).

[18] M. Halik, H. Klauk, U. Zschieschang, G. Schmid, W. Radlik, W. Weber. Polymer Gate Dielectrics and Conducting-Polymer Contacts for High-Performance Organic Thin-Film Transistors. *Adv. Mater.* **14**, 1717-1722 (2002).

[19] M. E. Roberts, S. C. B. Mannsfeld, N. Queralto, C. Reese, J. Locklin, W. Knoll, Z. Bao. Water-stable organic transistors and their application in chemical and biological sensors. *P. Natl. Acad. Sci.* **105**, 12134-12139 (2008).

[20] Y.-Y. Noh, H. Sirringhaus. Ultra-thin polymer gate dielectrics for top-gate polymer field-effect transistors. *Org. Electron.* **10**, 174-180 (2009).

[21] J. Collet, O. Tharaud, A. Chapoton, D. Vuillaume. Low-voltage, 30 nm channel length, organic transistors with a self-assembled monolayer as gate insulating films. *Appl. Phys. Lett.* **76**, 1941-1943 (2000).

[22] L. A. Majewski, R. Schroeder, M. Grell. Low-Voltage, High-Performance Organic Field-Effect Transistors with an Ultra-Thin TiO_2 Layer as Gate Insulator. *Adv. Funct. Mater.* **15**, 1017-1022 (2005).

[23] H. Klauk, U. Zschieschang, J. Pflaum, M. Halik. Ultralow-power organic complementary circuits. *Nature*, **445**, 745-748 (2007).

[24] J. Bobacka, A. Ivaska, M. Grzeszczuk. Electrochemical study of poly(3-octylthiophene) film electrodes II. Reversible redox/conductivity state switching. Impedance study. *Synth. Met.* **44**, 21-34 (1991).

[25] M. J. Panzer, C. D. Frisbie. High Carrier Density and Metallic Conductivity in Poly(3-hexylthiophene) Achieved by Electrostatic Charge Injection. *Adv. Funct. Mater.* **16**, 1051-1056 (2006).

[26] H. G. O. Sandberg, T. G. Bäcklund, R. Österbacka, H. Stubb. High-Performance All-Polymer Transistor Utilizing a Hygroscopic Insulator. *Adv. Mater.* **16**, 1112-1115 (2004).

[27] T. G. Bäcklund, R. Österbacka, H. Stubb, J. Bobacka, A. Ivaska. Operating principle of polymer insulator organic thin-film transistors exposed to moisture. *J. Appl. Phys.* **98**, 074504 (2005).

[28] L. Herlogsson, X. Crispin, N. D. Robinson, M. Sandberg, O.-J. Hagel, G. Gustafsson, M. Berggren. Low-Voltage Polymer Field-Effect Transistors Gated via a Proton Conductor. *Adv. Mater.* **19**, 97-101 (2007).

[29] J. H. Cho, J. Lee, Y. Xia, B. Kim, Y. He, M. J. Renn, T. P. Lodge, C. D. Frisbie. Printable ion-gel gate dielectrics for low-voltage polymer thin-film transistors on plastic. *Nat. Mater.* **7**, 900-906 (2008).

[30] J. D. Yuen, A. S. Dhoot, E. B. Namdas, N. E. Coates, M. Heeney, I. McCulloch, D. Moses, A. J. Heeger. Electrochemical Doping in Electrolyte-Gated Polymer Transistors. *J. Am. Chem. Soc.* **129**, 14367-14371 (2007).

[31] J. Lee, L. G. Kaake, J. H. Cho, X.-Y. Zhu, T. P. Lodge, C. D. Frisbie. Ion Gel-Gated Polymer Thin-Film Transistors: Operating Mechanism and Characterization of Gate Dielectric Capacitance, Switching Speed, and Stability. *J. Phys. Chem. C* **113**, 8972-8981 (2009).

[32] E. Said, X. Crispin, L. Herlogsson, S. Elhag, N. D. Robinson, M. Berggren. Polymer field-effect transistor gated via a poly(styrenesulfonic acid) thin film. *Appl. Phys. Lett.* **89**, 143507 (2006).

[33] E. W. Paul, A. J. Ricco, M. S. Wrighton. Resistance of Polyaniline Films as a Function of Electrochemical Potential and the Fabrication of Polyaniline-Base Microelectronic Devices. *J. Phys. Chem.* **89**, 1441-1447 (1985).

[34] J. W. Thackeray, H. S. White, M. S. Wrighton. Poly(3-methylthiophene)-Coated Electrodes: Optical and Electrical Properties as a Function of Redox Potential and Amplification of Electrical and Chemical Signals Using Poly(3-methylthiophene)-Based Microelectrochemical Transistors. *J. Phys. Chem.* **89**, 5133-5140 (1985).

[35] S. Chao, M. S. Wrighton. Solid-State Microelectrochemistry: Electrical Characteristics of a Solid-State Microelectrochemical Transistor Based on Poly(3-methylthiophene). *J. Am. Chem. Soc.* **109**, 2197-2199 (1987).

[36] S. Chao, M. S. Wrighton. Characterization of a "Solid-State" Polyaniline-Base Transistor: Water Vapor Dependent Characteristics of a Device Employing a Poly(vinyl alcohol)/Phosphoric Acid Solid-State Electrolyte. *J. Am. Chem. Soc.* **109**, 6627-6631 (1987).

[37] D. Ofer, R. M. Crooks, M. S. Wrighton. Potential Dependence of the Conductivity of Highly Oxidized Polythiophenes, Polypyrroles, and Polyaniline: Finite Windows of High Conductivity. *J. Am. Chem. Soc.* **112**, 7869-7879 (1990).

[38] D. Nilsson, N. Robinson, M. Berggren, R. Forchheimer. Electrochemical Logic Circuits. *Adv. Mater.* **17**, 353-358 (2005).

[39] A. Kumar, J. Sinha. Electrochemical Transistors for Applications in Chemical and Biological Sensing. In: D. A. Bernards, R. M. Owens, G. G. Malliaras (Eds.), Organic Semiconductors in Sensor Applications. Springer-Verlag. Berlin, Heidelberg, New York (2008) pp. 245-261.

[40] M. Berggren, R. Forchheimer, J. Bobacka, P.-O. Svensson, D. Nilsson, O. Larsson, A. Ivaska. PEDOT:PSS-Based Electrochemical Transistors for Ion-to-Electron Transduction and Sensor Signal Amplification. In: D. A. Bernards, R. M. Owens, G. G. Malliaras (Eds.), Organic Semiconductors in Sensor Applications. Springer-Verlag. Berlin, Heidelberg, New York (2008) pp. 263-280.

[41] M. Nikolou, G. G. Malliaras. Applications of Poly(3,4-Ethylenedioxythiophene) Doped With Poly(Styrene Sulfonic Acid) Transistors in Chemical and Biological Sensors. *Chem. Rec.* **8**, 13-22 (2008).

[42] R. Bollström, A. Määttänen, D. Tobjörk, P. Ihalainen, N. Kaihovirta, R. Österbacka, M. Toivakka, J. Peltonen. A multilayer coated fiber-based substrate suitable for printed functionality. *Org. Electron.* **10**, 1020-1023 (2009).

[43] H. Sirringhaus, N. Tessler, D. S. Thomas, P. J. Brown, R. H. Friend, In *Advances in Solid State Physics* Ed. B. Kramer, Friedr. Vieweg & Sohn: Braunschweig, Vol. 39, pp. 101-110 (1999).

[44] A. Salleo. Charge transport in polymeric transistors. *Mater. Today* **10**, 38-45 (2007).

[45] I. Osaka, R. D. McCullough. Advances in Molecular Design and Synthesis of Regioregular Polythiophenes. *Acc. Chem. Res.* **41**, 1202-1214 (2008).

[46] R. D. McCullough, R. D. Lowe. Enhanced electrical conductivity in regioselectively synthesized poly(3-alkylthiophenes). *J. Chem. Soc., Chem. Commun.* 70-72 (1992).

[47] H. Sirringhaus, P. J. Brown, R. H. Friend, M. M. Nielsen, K. Bechgaard, B. M. W. Langevald-Voss, A. J. H. Spiering, R. A. J. Janssen, E. W. Meijer, P. Herwig, D. M. de Leeuw. Two-dimensional charge transport in self-organized, high-mobility conjugated polymers. *Nature* **401**, 685-688 (1999).

[48] R. Österbacka, C. P. An, X. M. Jiang, Z. V. Vardeny. Two-Dimensional Electronic Excitations in Self-Assembled Conjugated Polymer Nanocrystals. *Science* **287**, 839-842 (2000).

[49] H. Sirringhaus, N. Tessler, D. S. Thomas, R. H. Friend. Integrated Optoelectronic Devices Based on Conjugated Polymers. *Science* **280**, 1741-1744 (1998).

[50] J.-F. Chang, B. Sun, D. W. Breiby, M. M. Nielsen, T. I. Sölling, M. Giles, I. McCulloch, H. Sirringhaus. Enhanced Mobility of Poly(3-hexylthiophene) Transistors by Spin-Coating from High-Boiling-Point Solvents. *Chem. Mater.* **16**, 4772-4776 (2004).

[51] M. Surin, P. Leclére, R. Lazzaroni, J. D. Yuen, G. Wang, D. Moses, A. J. Heeger, S. Cho, K. Lee. Relationship between the microscopic morphology and the charge transport properties in poly(3-hexylthiophene) field-effect transistors. *J. Appl. Phys.* **100**, 033712 (2006).

[52] T. Lehtinen, G. Sundholm, S. Holmberg, F. Sundholm, P. Björnbom, M. Bursell. Electrochemical characterization of PVDF-based proton conducting membranes for fuel cells. *Electrochim. Acta* **43**, 1881-1890 (1998).

[53] N. Walsby, M. Paronen, J. Juhanoja, F. Sundholm. Sulfonation of Styrene-Grafted Poly(vinylidene fluoride) Films. *J. Appl. Polym. Sci.* **81**, 1572-1580 (2001).

[54] N. J. Kaihovirta, D. Tobjörk, T. Mäkelä, R. Österbacka. Low-Voltage Organic Transistors Fabricated Using Reverse Gravure Coating on Prepatterned Substrates. *Adv. Eng. Mater.* **10**, 640-643 (2008).

[55] L.-L. Chua, P. K. H. Ho, H. Sirringhaus, R. H. Friend. Observation of Field-Effect Transistor Behavior at Self-Organized Interfaces. *Adv. Mater.* **16**, 1609-1615 (2004).

[56] F. Xue, Z. Liu, Y. Su, K. Varahramyan. Inkjet printed silver source/drain electrodes for low-cost polymer thin film transistors. *Microel. Eng.* **83**, 298-302 (2006).

[57] F. A. Yildrim, R. R. Schliewe, W. Bauhofer, R. M. Meixner, H. Goebel, W. Krautschneider. Gate insulators and interface effects in organic thin-film transistors. *Org. Electron.* **9**, 70-76 (2008).

[58] Y. Jung, R. J. Kline, D. A. Fischer, E. K. Lin, M. Heeney, I. McCulloch, D. M. DeLongchamp. The Effect of Interfacial Roughness on the Thin Film Morphology and Charge Transport of High-Performance Polythiophenes. *Adv. Funct. Mater.* **18**, 742-750 (2008).

[59] D. Tobjörk, N. J. Kaihovirta, T. Mäkelä, F. S. Pettersson, R. Österbacka. All-printed low-voltage organic transistors. *Org. Electron.* **9**, 931-935 (2008).

[60] Y. Xia, J. Cho, B. Paulsen, C. D. Frisbie, M. J. Renn. Correlation of on-state conductance with referenced electrochemical potential in ion gel gated polymer transistors. *Appl. Phys. Lett.* **94**, 013304 (2009).

[61] M. Hamedi, L. Herlogsson, X. Crispin, R. Marcilla, M. Berggren, O. Inganäs. Fiber-Embedded Electrolyte-Gated Field-Effect Transistors for e-Textiles. *Adv. Mater.* **21**, 573-577 (2009).

[62] K. A. Mauritz, R. B. Moore. State of Understanding of Nafion. *Chem. Rev.* **104**, 4535-4585 (2004).

[63] K. Schmidt-Rohr, Q. Chen. Parallell cylindrical water nanochannels in Nafion fuel-cell membranes. *Nat. Mater.* **7**, 75-83 (2008).

[64] O. Larsson, E. Said, M. Berggren, X. Crispin. Insulator Polarization Mechanisms in Polyelectrolyte-Gated Organic Field-Effect Transistors. *Adv. Funct. Mater.* **19**, 3334-3341 (2009).

[65] M. J. Panzer, C. D. Frisbie. Polymer Electrolyte-Gated Organic Field-Effect Transistors: Low-Voltage, High-Current Switches for Organic Electronics and Testbeds for Probing Electrical Transport at High Charge Carrier Density. *J. Am. Chem. Soc.* **129**, 6599-6607 (2007).

[66] P. M. Beaujuge, J. R. Reynolds. Color Control in π-Conjugated Organic Polymers for Use in Electrochromic Devices. *Chem. Rev.* **110**, 268-320 (2010).

[67] S. K. M. Jönsson, J. Birgerson, X. Crispin, G. Greczynski, W. Osikowicz, A. W. Denier van der Gon, W. R. Salaneck, M. Fahlman. The effects of solvents on the morphology and sheet resistance in poly(3,4-ethylenedioxythiophene)-polystyrenesulfonic acid (PEDOT-PSS) films. *Synth. Met.* **139**, 1-10 (2003).

[68] J. Ouyang, Q. Xu, C.-W. Chu, Y. Yang, G. Li, J. Shinar. On the mechanism of conductivity enhancement in poly(3,4-ethylenedioxythiophene):poly(styrene sulfonate) film through solvent treatment. *Polymer* **45**, 8443-8450 (2004).

[69] X. Crispin, F. L. E. Jakobsson, A. Crispin, P. C. M. Grim, P. Andersson, A. Volodin, C. van Haesendonck, M. Van der Auweraer, W. R. Salaneck, M. Berggren. The Origin of the High Conductivity of Poly(3,4-ethylenedioxythiophene)-Poly(styrenesulfonate) (PEDOT-PSS) Plastic Electrodes. *Chem. Mater.* **18**, 4354-4360 (2006).

[70] A. M. Nardes, M. Kemerink, M. M. de Kok, E. Vinken, K. Maturova, R. A. J. Janssen. Conductivity, work function, and environmental stability of PEDOT:PSS thin films treated with sorbitol. *Org. Electron.* **9**, 727-734 (2008).

[71] U. Barsch, F. Beck. Anodic overoxidation of polythiophenes in wet acetonitrile electrolytes. *Electrochim. Acta* **41**, 1761-1771 (1996).

[72] M. Lapkowski, A. Pron. Electrochemical oxidation of poly(3,4-ethylenedioxythiophene) – "in situ" conductivity and spectroscopic investigations. *Synth. Met.* **110**, 79-83 (2000).

[73] S. Möller, C. Perlov, W. Jackson, C. Taussig, S. R. Forrest. A polymer/semiconductor write-once read-many-times memory. *Nature* **426**, 166-169 (2003).

[74] E. Y. H. Teo, Q. D. Ling, Y. Song, Y. P. Tan, W. Wang, E. T. Kang, D. S. H. Chan, C. Zhu. Non-volatile WORM memory device based on an acrylate polymer with electron donating carbazole pendant groups. *Org. Electron.* **7**, 173-180 (2006).

[75] J. Lin, D. Ma. The morphology control of pentacene for write-once-read-many-times memory devices. *J. Appl. Phys.* **103**, 024507 (2008).

[76] E. Said, O. Larsson, M. Berggren, X. Crispin. Effects of the Ionic Currents in Electrolyte-gated Organic Field-Effect Transistors. *Adv. Funct. Mater.* **18**, 3529-3536 (2008).

[77] H. Harada, T. Fuchigami, T. Nonaka. Degradation and its prevention, and the deactivation and reactivation of electroactive polythiophene films during oxidation/reduction cycles. *J. Electroanal. Chem.* **303**, 139-150 (1991).

[78] N. Ljungqvist, T. Hjertberg. Oxidative Degradation of Poly(3-octylthiophene). *Macromolecules* **28**, 5993-5999 (1995).

[79] P. Tehrani, A. Kanciurzewska, X. Crispin, N. D. Robinson, M. Fahlman, M. Berggren. The effect of pH on the electrochemical over-oxidation in PEDOT:PSS films. *Solid State Ionics* **177**, 3521-3527 (2006).

[80] R. F. Grossman. Antioxidants. In: J. T. Lutz, Jr., R. F. Grossman (Eds.), Polymer Modifiers and Additives. Marcel Dekker, Inc. New York, NY (2001) pp. 1-34.

[81] M. Manceau, A. Rivaton, J.-L. Gardette, S. Guillerez, N. Lemaitre. The mechanism of photo- and thermooxidation of poly(3-hexylthiophene) (P3HT) reconsidered. *Polym. Degrad. Stabil.* **94**, 898-907 (2009).

[82] B. A. Mattis, P. C. Chang, V. Subramanian. Performance recovery and optimization of poly(3-hexylthiophene) transistors by thermal cycling. *Synt. Met.* **156**, 1241-1248 (2006).

SVENSK RESUMÉ

I likhet med konventionella polymerer (plaster) är de π-konjugerade polymererna flexibla, lösliga och processbara vid låga temperaturer (< 150 ^{o}C). Därutöver har de egenskapen att leda ström. Konduktivitetsintervallet är brett och omfattar nästintill metallisk ledningsförmåga å ena sidan, via halvledarkonduktiva till isolerande å andra sidan. Polymererna utgörs av regelbundna kedjor av kolatomer och associeras sålunda till organiska material. Sedan de första vetenskapliga rapporterna publicerades vid slutet av 1970-talet har π-konjugerade polymerer använts och utvecklats i flera elektroniska tillämpningar såsom solceller, dioder, lysdioder och transistorer. Nobelpriset i kemi tilldelades år 2000 åt Hideki Shirakawa, Alan J. Heeger och Alan G. MacDiarmid för upptäckten och utvecklandet av ledande polymerer.

I min avhandling har jag arbetat med att utveckla och förstå lågspännings jonmodulerade organiska transistorer. I avhandlingen behandlas två typer av jonmodulerade organiska transistorer: (1) den jonmodulerade organiska fälteffekt transistorn (jonmodulerade OFETen), som utgör den centrala transistorn i avhandlingen, samt (2) den elektrokemiska transistorn (ECTn). Den första typen fungerar som en konventionell OFET. Den elektroniska strömmen i halvledaren moduleras av det elektriska fältet över isolatorn. Med användandet av en elektrolyt ”isolator” orsakar polariseringen av jonerna däremot ett högt elektriskt fält vid elektrolyt/halvledargränssnittet och man åstadkommer modulering av strömmen redan vid en volts drivspänningar. I den andra typen utnyttjas reversibel elektrokemi för att modulera strömmen. Vid låga spänningar (omkring en volt) tränger joner in i den elektriskt aktiva polymeren för att medelst reduktion/oxidation modulera strömmen. Ett viktigt ändamål har också varit att kunna tillverka transistorerna med masstillverkningsmetoder, vilket möjliggörs med polymerernas egenskaper.

Avhandlingen är delvis en fortsättning på det tidigare vetenskapliga arbetet som gjordes på HIFETen (Hygroscopic Insulator Field-Effect Transistor) vid institutionen för fysik vid ÅA. HIFETen utnyttjar den jonledande hygroskopiska polymeren poly(vinyl fenol) för att modulera strömmen i halvledaren. Den fortsatta målsättningen var att tillverka fungerande HIFETar med masstillverkningsmetoder. För konventionella

OFETer är det känt att övergången till grova substrat (såsom plast och papper) har försämrande effekter på transistorfunktionen. Grova substrat är dock oundvikliga ifall man ämnar tillverka flexibel elektronik på ett kostnadseffektivt sätt. I avhandlingen har HIFETen studerats för att klargöra att jonmodulerade OFETer påverkas mindre utav övergången till grövre plastsubstrat jämfört med OFETer. Med den kunskapen har vi sedermera presenterat lågspännings HIFETar tillverkade med masstillverkningsmetoder på såväl plast- som på papperssubstrat.

Lejonparten av avhandlingen fokuseras på jonmodulerade organiska transistorer som utnyttjar jonledande polymera membran. Membranen har vanligtvis tillämpats i bränslecells-, gas och vätskeseparerings- samt i kloralkali-industrin. I avhandlingen visas dock att membranet även fungerar som substrat och som elektrolyt för en eller flera komponenter. MemFETen (Membrane based Field-Effect Transistor) utgör modelltransistorn men även den helpolymera och membran baserade ECTn demonstreras. I avhandlingens senare del studeras fuktens roll i elektrolyten och hur den påverkar transistorbeteendet. Samtliga elektrolyter i avhandlingen (inklusive poly(vinyl fenolen)) behöver fukt för att kunna leda joner. MemFETen används i studierna och fuktens reversibla och irreversibla inverkan på den polymera halvledaren klargörs även med hjälp av spektroskopiska tekniker. För att förhindra den irreversibla degraderingen av den polymera halvledaren presenteras steriskt hindrade fenoliska antioxidanter som ett intressant alternativ.

Avhandlingen klargör skillnaderna mellan OFETen, jonmodulerade OFETen och ECTn. De jonmodulerade organiska transistorernas möjlighet att framställas med masstillverkningsmetoder presenteras. Nya koncept introduceras och svagheter identifieras. Arbetet skall däremot inte anses slutfört utan forskningen fortgår för att kringgå svagheterna, öka på transistorernas stabilitet och framförallt tillämpa dem i innovativa applikationer.

ISBN 978-952-12-2468-3
Painosalama Oy, Turku, Finland 2010